Neural Evolution Strategy for Black-box Pareto Set Learning

Chengyu Lu^{1,2}, Zhenhua Li^{3,4,*}, Xi Lin^{1,2}, Ji Cheng^{1,2}, Qingfu Zhang^{1,2,*}

¹ City University of Hong Kong, ² City University of Hong Kong Shenzhen Research Institute

³ Nanjing University of Aeronautics and Astronautics

⁴ MIIT Key Laboratory of Pattern Analysis and Machine Intelligence

{chengyulu3-c, xi.lin, J.Cheng}@my.cityu.edu.hk, zhenhua.li@nuaa.edu.cn
qingfu.zhang@cityu.edu.hk

Abstract

Multi-objective optimization problems (MOPs) are prevalent in numerous real-world applications. Recently, Pareto Set Learning (PSL) has emerged as a powerful paradigm for solving MOPs. PSL can produce a neural network for modeling the set of all Pareto optimal solutions. However, applying PSL to black-box objectives, particularly those exhibiting non-separability, high dimensionality, and/or other complex properties, remains very challenging. To address this issue, we propose leveraging evolution strategies (ESs), a class of specialized black-box optimization algorithms, within the PSL paradigm. Traditional ESs capture the complex dimensional dependencies less efficiently, which can significantly hinder their performance in PSL. To tackle this issue, we suggest encapsulating the dependencies within a neural network, which is then trained using a novel gradient estimation method. The proposed method, termed Neural-ES, is evaluated using a bespoke benchmark suite for black-box PSL. Experimental comparisons with other methods demonstrate the efficiency of Neural-ES, underscoring its ability to learn the Pareto sets of challenging black-box MOPs.

1 Introduction

Many real-life applications need to consider multiple conflicting objectives simultaneously [1–3]. Since these objectives can rarely be optimized by a single solution simultaneously, a commonly used approach is to find the *Pareto set* (PS) [4], which contains all solutions with different optimal tradeoffs among the objectives. Traditional methods [5–8] approximate the PS using only a finite number of solutions, risking not aligning with users' trade-off preferences determined after optimization.

Recently, a novel paradigm called *Pareto Set Learning* (PSL) has attracted increasing attention [9–15]. PSL formulates a multi-objective optimization problem (MOP) [4] as a set learning task by decomposing the problem into an *infinite* number of single-objective subproblems and resolving the optimal solutions for all of them. In this process, a *set model*, typically a neural network, learns the mapping from an input preference to its corresponding Pareto optimal solution. Consequently, the Pareto set is recovered in both the objective and solution spaces. Unlike traditional multi-objective methods, which only accommodate a limited number of predefined user preferences [16, 5], a trained PSL model can provide a tailored optimal solution for any valid decision-maker preference trade-off without requiring re-optimization from scratch.

Despite the rapid development of PSL, it remains largely unclear how to apply this paradigm to a black-box MOP where both the analytic expression and derivatives of the objectives are unknown. On

^{*}Correspondence to: Qingfu Zhang and Zhenhua Li

one hand, black-box objectives are prevalent in practice [17, 18, 7], making it imperative to develop novel approaches for effectively tackling black-box MOPs. On the other hand, when exhibiting common properties such as non-separability and high dimensionality, black-box objectives can become highly challenging, rendering their resolution an open question. Moreover, since PSL involves solving numerous subproblems that may themselves be black boxes, jointly optimizing them poses a significantly greater challenge than solving a single black-box optimization problem. Lin *et al.* [9] proposed integrating a Gaussian process model into PSL for solving expensive MOPs. However, Gaussian process models scale poorly with problem dimensions and increased evaluation budgets, which may be less suited for more general black-box MOPs.

Evolution Strategy (ES) has remained one of the most successful black-box optimization algorithms for decades [19–21]. An ES algorithm utilizes a distribution model, typically a multivariate Gaussian distribution, to search in complex fitness landscapes. Key elements that govern a competitive ES algorithm include an adaptive covariance matrix, the resemblance to gradient search, and sophisticated adaptation strategies. Compared to other zeroth-order optimization methods that sample solutions from isotropic distributions [22, 23], ESs excel at dealing with variables' complex *dimensional dependencies*, a prevalent feature as well as a significant challenge in real-world optimization problems [24–26]. It is natural to integrate PSL with ES for black-box multi-objective optimization. On one hand, PSL decomposes an MOP into single-objective subproblems, aligning perfectly with the strengths of ES. On the other hand, ES's search efficiency paves the way for dealing with challenging black-box objectives. However, traditional ES algorithms experience high computational complexity [27, 28] and rely heavily on adaptation strategies [29–31]. These limitations are particularly crucial and evident within PSL, as they can lead to failures in decoupling dimensional dependencies and significantly hinder the performance of ES.

To enhance the PSL paradigm for solving black-box MOPs, we propose a novel method called Neural-ES, which acts as the back-end of the set model. To effectively handle dimensional dependencies, we propose rethinking the way ES algorithms decouple such dependencies. Rather than leveraging a covariance matrix, Neural-ES encapsulates the dependencies within a neural network. To be more specific, we partition the high-dimensional design variable of a black-box objective into lower-dimensional segments. Each segment follows a distinct multivariate Gaussian distribution. The network, which also acts as the set model, parameterizes the distribution conditioned on all previously sampled segments. To train the network, we estimate the gradient in a novel way closely related to the natural gradient [32]. Neural-ES is well-suited for black-box tasks involving neural networks, with PSL serving as a typical example. We summarize our contributions in threefold:

- We propose Neural-ES, a novel algorithm that utilizes a neural network to capture complex dimensional dependencies effectively, which enhances the versatility of the ES repertoire.
- We establish a novel PSL formulation for black-box MOPs, which enables the use of efficient derivative-free optimization algorithms to address the problem efficiently.
- We conduct extensive experiments using a novel benchmark suite designed for evaluating black-box PSL problems. Results demonstrate that Neural-ES effectively addresses nonseparable MOPs. To the best of our knowledge, we are the first to scale the PSL paradigm to over 1,000 dimensions in black-box scenarios.

2 Preliminaries & related works

2.1 Multi-objective optimization

A continuous MOP (MOP) [4] is defined as:

$$\underset{\boldsymbol{x} \in \mathcal{X}}{\text{minimize}} \, \boldsymbol{F}(\boldsymbol{x}) = (f_1(\boldsymbol{x}), ..., f_M(\boldsymbol{x}))^T, \tag{1}$$

where $F: \mathcal{X} \to \mathbb{R}^M$ consists of M objectives $f_i: \mathcal{X} \to \mathbb{R}$ for all i=1,...,M. In many cases, the objectives conflict with each other, and a single solution cannot optimizes all of them simultaneously. An alternative is to pursue the *Pareto set*, which consists of optimal solutions under all possible trade-offs among the objectives. Collectively, these solutions exclude any opportunity to improve one objective without compromising at least one other. We provide formal definitions of the fundamentals of MOPs in the following:

Definition 1 (Pareto dominance). Let $x, x' \in \mathcal{X}$ be two solutions to (1), x' is said to dominate x, denoted by $x' \prec x$, if $f_i(x') \leq f_i(x)$, $\forall i = 1, ..., M$, and $f_i(x') < f_i(x)$, $\exists j = 1, ..., M$.

Definition 2 (Pareto optimality). A solution $x \in \mathcal{X}$ is Pareto optimal if $x' \not\prec x$, $\forall x' \in \mathcal{X}$.

Definition 3 (Pareto set & front). The set of all the Pareto optimal solutions is called the Pareto set, denoted by $PS = \{ \boldsymbol{x} \in \mathcal{X} | \nexists \boldsymbol{x}', \boldsymbol{x}' \prec \boldsymbol{x} \}$; the image of PS in the objective space is called the Pareto front, denoted by $PF = \{ \boldsymbol{F}(\boldsymbol{x}) | \boldsymbol{x} \in PS \}$.

Multi-objective evolutionary algorithms (MOEAs) MOEAs have developed as one of the key methodologies for solving MOPs [16, 5, 6]. Compared to other methodologies [33, 7], MOEAs approximate the PS by a population of diverse non-dominated solutions, without collapsing into a single point. Several highly efficient MOEA variants have been developed [6, 34, 35]. However, MOEAs encounter longstanding issues, including inefficient Pareto ranking, misalignment with decision-makers' preferences, poor scalability in relation to population size, and ineffective information sharing among subproblems.

2.2 Pareto set learning

PSL formulates an MOP as follows. First, given a preference vector $\boldsymbol{\alpha}=(\alpha_1,...,\alpha_M)^T\in\Delta_M$ where $\Delta_M=\{\boldsymbol{\alpha}\in\mathbb{R}_+^M|\mathbf{1}^T\boldsymbol{\alpha}=1\}$ is the (M-1)-dimensional simplex, and an aggregation function $g:\mathbb{R}^M\to\mathbb{R}$ conditioned on $\boldsymbol{\alpha}$, (1) can be aggregated into a single-objective subproblem. Under some mild conditions, solving every possible subproblem conditioned on all possible $\boldsymbol{\alpha}$ recovers the entire Pareto set. Then, an MOP in (1) can be formulated as:

$$\underset{\boldsymbol{\theta} \in \Theta}{\operatorname{minimize}} \mathbb{E}_{\boldsymbol{\alpha} \sim \mathcal{U}(\Delta_M)}[g(\boldsymbol{x}; \boldsymbol{\alpha})], \text{ where } \boldsymbol{x} = \boldsymbol{\varphi}_{\boldsymbol{\theta}}(\boldsymbol{\alpha}), \tag{2}$$

where Θ is the parameter space, $\mathcal{U}(\Delta_M)$ denotes a probability distribution (in this work, it is set as a uniform distribution) over Δ_M , and $\varphi_{\theta}:\Delta_M\to\mathcal{X}$ is called a *set model* parameterized by θ . In the ideal case, $\varphi_{\theta}(\alpha)=\operatorname{argmin}_{\boldsymbol{x}\in\mathcal{X}}g(\boldsymbol{x};\alpha), \forall \alpha\in\Delta_M$, which means φ_{θ} maps each preference to its corresponding Pareto optimal solution that minimizes $g(\cdot;\alpha)$.

Recent developments Since its inception, PSL [9] has been rapidly applied to various problem types, including expensive [13, 11], combinatorial [36], and smooth MOPs [37]. However, these methods face challenges with general black-box MOPs, particularly when the objectives are high-dimensional and exhibit complex dimensional dependencies. Lin *et al.* [15] contributed a primary work called evolutionary-PSL (EPSL), where a finite difference approach is employed to train the set model. However, due to the absence of a comprehensive distribution model, most existing derivative-free PSL algorithms have been validated only on low-dimensional toy problems, leaving their performance on challenging problems uncertain.

2.3 Evolution strategy

ES is a prominent class of derivative-free optimization algorithms. Popular algorithms include natural evolution strategy (NES) [28, 20], the state-of-the-art covariance matrix adaptation (CMA-ES) [19, 27], and the also competitive but more time-efficient matrix adaptation evolution strategy (MA-ES) [38]. An ES algorithm first formulates a general black-box optimization problem in question as:

$$\underset{\boldsymbol{x} \in \mathcal{X}}{\operatorname{minimize}} f(\boldsymbol{x}) \Rightarrow \underset{\boldsymbol{\varphi} \in \Phi}{\operatorname{maximize}} - \mathbb{E}_{\pi(\boldsymbol{x}; \boldsymbol{\varphi})} \left[f(\boldsymbol{x}) \right], \tag{3}$$

where $\mathcal{X}\subseteq\mathbb{R}^n$ is the search space, $\pi(\boldsymbol{x};\boldsymbol{\varphi})$ is the probability density function, p.d.f., of a smooth distribution $\boldsymbol{x}\sim\pi(\boldsymbol{\varphi})$ parameterized by $\boldsymbol{\varphi}$, and Φ is the parameter space of $\boldsymbol{\varphi}$. At each $x\in\mathcal{X}$, only its f function value f(x) is available. Most commonly, $\pi(\boldsymbol{\varphi})=\mathcal{N}(\boldsymbol{m},\boldsymbol{C})$ is a multivariate Gaussian distribution where $\boldsymbol{\varphi}$ consists of the distribution mean $\boldsymbol{m}\in\mathbb{R}^n$ and the covariance matrix $\boldsymbol{C}\in\mathbb{S}^n_{++}$ (where \mathbb{S}^n_{++} denotes the space of n-dimensional symmetric and positive definite matrices). In brief, an ES optimizes f by 1) sampling random samples from $\pi(\boldsymbol{\varphi})$ and 2) effectively updating $\boldsymbol{\varphi}$.

Covariance matrix and dimensional dependencies It is widely acknowledged that the covariance matrix plays a vital role in the performance of an ES algorithm. Hansen *et al.* [24] systematically

showed that CMA-ES, aided by an adaptive covariance matrix, effectively decouples the interacting problem dimensions. Beyer [26] showed that the covariance matrix decouples the dimensional dependencies by effectively converging to the inverse of a convex objective's Hessian. Both Akimoto *et al.* [39] and Glasmarchers *et al.* [28] demonstrated that the rank- μ of CMA-ES amounts to the natural gradient ascent method. The ability to decouple dimensional dependencies positions NES and CMA-ES as second-order quasi-Newton methods rather than merely being zeroth-order finite-difference methods.

Adaptation strategies In addition to natural gradient, refined adaptation strategies also contribute to the competitiveness of ESs, as exemplified by cumulative step-length control and evolution paths [19, 40]. An evolution path accumulates the movement trajectories of the distribution over time, thereby exploiting a promising search direction. Evidence suggests that ESs leveraging both natural gradient and adaptation strategies significantly outperform those that rely solely on natural gradient [28, 29].

3 Black-box Pareto set learning

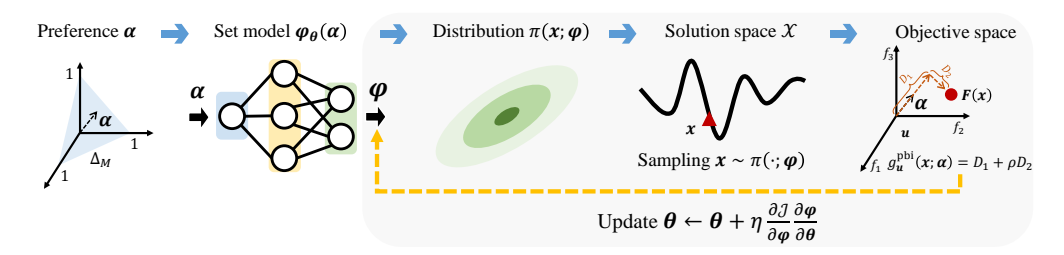


Figure 1: Black-box PSL formulation. The blue arrows indicate the forward process, and the yellow arrow indicates the gradient back-propagation; the shadowed area is where an ES participates and is referred to as the *back-end* of the set model.

3.1 Problem formulation

A black-box MOP refers to those F in (1) that provide no information beyond the objective values of a solution. In this case, we formulate (2) through the *reparameterization* trick:

$$\underset{\boldsymbol{\theta} \in \Theta}{\operatorname{maximize}} \, \mathcal{J}(\boldsymbol{\theta}) = \mathbb{E}_{\boldsymbol{\alpha} \sim \mathcal{U}(\Delta_M)} \mathbb{E}_{\pi(\boldsymbol{x}; \boldsymbol{\varphi})}[-g(\boldsymbol{x}; \boldsymbol{\alpha})], \text{ where } \boldsymbol{\varphi} = \boldsymbol{\varphi}_{\boldsymbol{\theta}}(\boldsymbol{\alpha}). \tag{4}$$

The above formulation (4) distinguishes itself from (2) in the nested expectation. Instead of outputting x directly, the set model $\varphi_{\theta}(\alpha)$ first maps a preference vector α to a distribution $\pi(\varphi)$ parameterized by $\varphi = \varphi_{\theta}(\alpha)$, and then samples solutions from the distribution. To train the set model, an ES is employed to sample solutions and estimate gradients. When θ is perfectly learned, regarding an arbitrary α , a random $x \sim \pi(\varphi_{\theta}(\alpha))$ converges in probability to the minimum of $g(\cdot; \alpha)$.

To further illustrate this process, we outline the paradigm of black-box PSL in Fig. 1. First, a random preference vector $\boldsymbol{\alpha} \sim \mathcal{U}(\Delta_M)$ is sampled and inputted into the set model $\varphi_{\boldsymbol{\theta}}$. The set model subsequently outputs a parameter vector $\boldsymbol{\varphi} \in \Phi$, which parameterizes a distribution $\pi(\boldsymbol{x}; \boldsymbol{\varphi})$. A random solution $\boldsymbol{x} \sim \pi(\boldsymbol{\varphi})$ is then sampled from this distribution and evaluated on the specific $g(\cdot; \boldsymbol{\alpha})$. Here, we use the PBI aggregation function $g_{\boldsymbol{u}}^{\text{pbi}}$ [8] as an example. When we have sampled enough $\boldsymbol{\alpha}$ s, and for each $\boldsymbol{\alpha}$ there have been several samples \boldsymbol{x} s, we can estimate the gradient and back-propagate it to $\boldsymbol{\theta}$ through the chain rule.

3.2 Key challenges

The formulation (4) introduces several challenges for ES. First, the high computational complexity of the covariance matrix significantly impedes an ES's performance. It takes $\Theta(n^2)$ space complexity of the set model to generate a covariance matrix, and $\Theta(n^4)$ time complexity or even more to compute the gradient, which will soon become prohibitive as n increases. Even worse, since each distribution φ corresponds to a different α , as can be seen from Fig. 1, the large number of decomposed subproblems

in PSL necessitates an equally large number of covariance matrices, which drastically increases the learning burden of the set model.

Second, it is difficult, if not impossible, to apply sophisticated adaptation strategies in PSL problems. These strategies are known to accelerate convergence by counteracting the slow-changing rate suppressed by the Kullback-Leibler (KL)-divergence [26]. Despite some recent findings [41], the connection between these strategies and gradient search remains unclear, which limits their use in training the set model. Furthermore, as there are numerous decomposed subproblems in a PSL problem, it is infeasible to track a different evolution path for each subproblem.

The above characteristics of a black-box PSL problem make the direct integration of ESs rarely yield competitive performance, posing new challenges for ESs to learn in a typical adaptation-free scenario.

4 Neural evolution strategy

4.1 Basic idea

Consider a general single-objective problem: maximize θ $\bar{\mathcal{J}}_{\alpha}(\theta) = \mathbb{E}_{\pi(\boldsymbol{x};\boldsymbol{\varphi})}[f(\boldsymbol{x})]$, where $\boldsymbol{\varphi} = \boldsymbol{\varphi}_{\theta}(\alpha)$, α is a problem specific parameter, and $\boldsymbol{x} \in \mathbb{R}^n$. Assuming $n = p \times d$ where p and d are positive integers, \boldsymbol{x} can be partitioned into p segments each of length d, as follows:

$$\boldsymbol{x} = (\underbrace{\mathbf{x}_{1}, ..., \mathbf{x}_{d}}_{\boldsymbol{x}_{1}^{T}}, ..., \underbrace{\mathbf{x}_{(i-1)d+1}, ..., \mathbf{x}_{id}}_{\boldsymbol{x}_{p}^{T}}, ..., \underbrace{\mathbf{x}_{n-d+1}, ..., \mathbf{x}_{n}}_{\boldsymbol{x}_{p}^{T}})^{T}$$

$$(5)$$

By conditional probability, $\pi(x; \varphi) = \pi(x; \varphi_{\theta}(\alpha))$ can be decomposed into the product of a chain of *p.d.f.*s each concerning a different x_i , and conditioned on all the previous $x_0, x_1, ..., x_{i-1}$:

$$\pi(\boldsymbol{x}; \boldsymbol{\varphi}_{\boldsymbol{\theta}}(\boldsymbol{\alpha})) = \prod_{i=1}^{p} \mathcal{N}_{\boldsymbol{\theta}}(\boldsymbol{x}_{i} | \underbrace{\boldsymbol{x}_{0}, \boldsymbol{x}_{1}, ..., \boldsymbol{x}_{i-1}}_{\boldsymbol{x}_{0:i-1}}) = \prod_{i=1}^{p} \mathcal{N}\left(\boldsymbol{x}_{i}; \boldsymbol{\varphi}_{\boldsymbol{\theta}}(\boldsymbol{x}_{0:i-1})\right). \tag{6}$$

With a slight abuse of symbols, we redefine $\varphi_{\theta}: \bigcup_{i=1}^n \mathbb{R}^i \to \mathbb{R}^d \times \mathbb{S}^d_{++}$ hereafter, which means φ_{θ} maps variable-length inputs to the parameters of a d-dimensional Gaussian. More specifically, an input $x_{0:i-1}$ consists of all the segments $x_0, x_1..., x_{i-1}$ preceding x_i , and the output $\varphi_{\theta}(x_{0:i-1})$ consists of the mean $m_{\theta}(x_{0:i-1}) \in \mathbb{R}^d$ and the covariance matrix $C_{\theta}(x_{0:i-1}) \in \mathbb{S}^d_{++}$. x_0 is just an alias of α , for notation consistency. (6) directly models the dependency of x_i on $x_{0:i-1}$ as the mapping φ_{θ} . In practice, φ_{θ} is a neural network. Fig. 2 illustrates the idea.

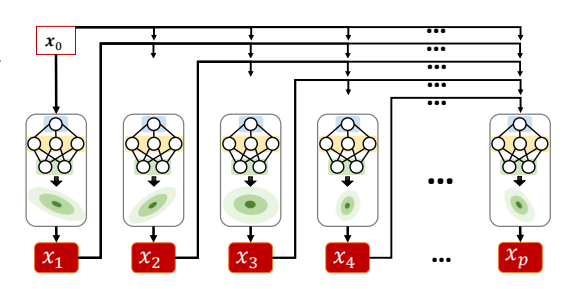


Figure 2: An illustration of using (6) to sample a random solution $x \sim \pi(\varphi_{\theta}(\alpha))$.

As the Gaussian is smooth w.r.t. φ , the network

 θ can be trained by gradient ascent. A conceptual algorithm is inspired, which iteratively 1) sample λ solutions $\{x^j\}_{j=1}^{\lambda}$ from $\pi_{\theta}(\cdot;\varphi)$ independently, and 2) estimate the gradient using these samples and back-propagate to θ until convergence.

4.2 Implementation

4.2.1 Designing the covariance matrix

For any $i \in [p]$, a full covariance matrix $C_{\theta}(x_{0:i-1})$ of $\Theta(d^2)$ degrees of freedom necessitates $\Theta(d^2)$ output neurons to generate it and $\Theta(d^2)$ time complexity to sample solutions as well as to estimate its gradient. To reduce the overall complexity to $\Theta(n)$, the above must be reduced to $\Theta(d)$.

As is a common trick in ES variants for high-dimensional tasks [42, 29, 30], we can replace a full covariance matrix by a *rank-one model*. More specifically, we define a step-size $\sigma_{\theta}(\mathbf{x}_{0:i-1}) > 0$ and a component $\mathbf{v}_{\theta}(\mathbf{x}_{0:i-1}) \in \mathbb{R}^d$, then $C_{\theta}(\mathbf{x}_{0:i-1})$ can be parameterized by:

$$C_{\theta}(x_{0:i-1}) = \sigma_{\theta}^{2}(x_{0:i-1}) \left(I + v_{\theta}(x_{0:i-1}) v_{\theta}(x_{0:i-1})^{T} \right).$$
 (7)

Of the above, σ_{θ} controls the isotropic variance of the samples, and v_{θ} is expected to identify a promising search direction. Although the number of free parameters in $C_{\theta}(x_{0:i-1})$ decreases, $\pi(\varphi)$ suffices to decouple complex dimensional dependencies when p is large enough. By this means, the space complexity of θ 's output layer is reduced to $\Theta(d)$.

Following (7), a solution is practically generated by:

$$x_i = m_{\theta}(x_{0:i-1}) + \sigma_{\theta}(x_{0:i-1})(z + rv_{\theta}(x_{0:i-1})),$$
 (8)

where $z \sim \mathcal{N}(\mathbf{0}, \mathbf{I})$, $z \in \mathbb{R}^d$, and $r \sim \mathcal{N}(0, 1)$. After p iterations, an $x \sim \pi_{\theta}(\cdot; \alpha)$ is recovered by stacking the $x_1, ..., x_p$. The time complexity of (8) is $\Theta(d)$.

4.2.2 Revising the gradient

The gradient of θ can be derived as

$$\nabla \bar{\mathcal{J}}_{\alpha}(\boldsymbol{\theta}) = \sum_{i=1}^{p} \mathbb{E}_{\pi(\boldsymbol{x};\boldsymbol{\varphi})} \left[f(\boldsymbol{x}) \frac{\partial}{\partial \boldsymbol{\theta}} \left(\frac{\partial \ln \mathcal{N}(\boldsymbol{x}_{i}; \boldsymbol{\varphi}_{\boldsymbol{\theta}}(\boldsymbol{x}_{0:i-1}))}{\partial \boldsymbol{\varphi}_{\boldsymbol{\theta}}(\boldsymbol{x}_{0:i-1})} \right) \right]. \tag{9}$$

However, the partial derivative $\partial \ln \mathcal{N}(x_i; \varphi_{\theta}(x_{0:i-1}))/\partial \varphi_{\theta}(x_{0:i-1})$ rarely yields stable convergence behaviors of the mean $m_{\theta}(x_{0:i-1})$, because the shrinking of $C_{\theta}(x_{0:i-1})$ in turns stretches the gradient of $m_{\theta}(x_{0:i-1})$, preventing it from staying in stationary points. See [20, 26] as well as Section B.2 for more details.

To regulate the gradient, a remedy is to multiply each partial derivative in (9) by the inverse of the Fisher information matrix (a.k.a. the "Fisher") of $\varphi_i = \varphi_{\theta}(x_{0:i-1})$, which yields:

$$\tilde{\nabla} \bar{\mathcal{J}}_{\alpha}(\boldsymbol{\theta}) := \sum_{i=1}^{p} \mathbb{E}_{\pi(\boldsymbol{x};\boldsymbol{\varphi})} \left[f(\boldsymbol{x}) \frac{\partial}{\partial \boldsymbol{\theta}} \left(\boldsymbol{\mathcal{F}}(\boldsymbol{\varphi}_{i})^{-1} \frac{\partial \ln \mathcal{N}(\boldsymbol{x}_{i}; \boldsymbol{\varphi}_{\boldsymbol{\theta}}(\boldsymbol{x}_{0:i-1}))}{\partial \boldsymbol{\varphi}_{\boldsymbol{\theta}}(\boldsymbol{x}_{0:i-1})} \right) \right], \tag{10}$$

where $\mathcal{F}(\varphi_i) = \mathbb{E}_{\mathcal{N}(\boldsymbol{x}_i';\varphi_i)}[\nabla_{\varphi_i} \ln \mathcal{N}(\boldsymbol{x}_i';\varphi_i)\nabla_{\varphi_i} \ln \mathcal{N}(\boldsymbol{x}_i';\varphi_i)^T]$. The interpretation is that the Fisher penalizes drastic changes of the search distribution, counteracts the effect of the shrinking covariance, and thus guarantees stable convergence. More intrinsically, the following connects (10) to the natural gradient, which incorporates second-order information and is the steepest ascent direction on Riemannian manifolds [32].

Lemma 1. Consider a distribution $\pi(\varphi)$ with fixed parameters $\varphi = (\varphi_1^T, ..., \varphi_p^T)^T$ and a random sample $\mathbf{x} \sim \pi(\varphi)$. The partial derivative $\sum_{i=1}^p [\mathcal{F}(\varphi_i)^{-1}\partial \ln \mathcal{N}(\mathbf{x}_i; \varphi_i)/\partial \varphi_i]$ in (10) is an unbiased estimator for the natural gradient of the log-likelihood $\ln \pi(\mathbf{x}; \varphi)$ regarding φ .

Furthermore, empirical and theoretical evidence [20, 25, 26] have shown that unscaled objective values often lead to degenerated search distributions and premature convergence, due to the irregularity of f. ES algorithms alleviate this issue by replacing f(x) with rank-dependent weight values. Specifically, consider a set of objective values $\{f(x^j)\}_{j=1}^{\lambda}$ arranged in descending order, which means $f(x^1) \geq ... \geq f(x^{\lambda})$, we replace each $f(x^j)$ by w_j where $w_1 \geq ... \geq w_{\lambda}$. In this paper, we define $w_j = \ln\left(\left\lfloor \frac{\lambda}{2} \right\rfloor + \frac{1}{2}\right) - \ln j$.

According to Akimoto *et al.* [39], the Fisher $\mathcal{F}(\varphi_i)$ can be absorbed into the gradient without explicitly computing its inverse. Eventually, the gradient estimator based on a set of solutions $\{x^j\}_{j=1}^{\lambda}$ can be derived as:

$$\tilde{\nabla} \bar{\mathcal{J}}_{\alpha}(\boldsymbol{\theta}) \approx \frac{1}{\lambda} \sum_{i=1}^{p} \sum_{j=1}^{\lambda} w_{j} \begin{bmatrix} \boldsymbol{J}(\boldsymbol{m}_{ij})^{T} (\boldsymbol{x}_{i}^{j} - \boldsymbol{m}_{ij}) + \\ 2\sigma_{ij} (\|\boldsymbol{y}_{ij}\|^{2} + (\boldsymbol{v}_{ij}^{T} \boldsymbol{y})^{2} - \sigma_{ij}^{2} (d + 2\|\boldsymbol{v}_{ij}\|^{2} + \|\boldsymbol{v}_{ij}\|^{4})) \frac{\partial \sigma_{ij}}{\partial \boldsymbol{\theta}} + \\ \sigma_{ij}^{2} \boldsymbol{J} (\boldsymbol{v}_{ij})^{T} ((\boldsymbol{v}_{ij}^{T} \boldsymbol{y}_{ij}) \boldsymbol{y}_{ij} + \|\boldsymbol{y}_{ij}\|^{2} \boldsymbol{v} - 2\sigma_{ij}^{2} (1 + \|\boldsymbol{v}_{ij}\|^{2}) \boldsymbol{v}_{ij}) \end{bmatrix}, (11)$$

where $m_{ij} = m_{\theta}(x_{0:i-1}^j)$, $\sigma_{ij} = \sigma_{\theta}(x_{0:i-1}^j)$, $v_{ij} = v_{\theta}(x_{0:i-1}^j)$, $y_{ij} = x_i^j - m_{ij}$, $J(\cdot)$ computes the $d \times |\theta|$ dimensional Jacobian matrix of an input vector w.r.t. θ , and $\|\cdot\|$ computes the ℓ_2 -norm. We leave the tedious derivation steps in Section B.4. Each term irrelevant to θ (i.e., those except $J(m_{ij})$, $\partial \sigma_{ij}/\partial \theta$ and $J(v_{ij})$) yields $\Theta(d)$ time complexity.

4.3 The algorithm

We present Neural-ES in Alg. 1. During each epoch, i.e., lines 2 to 8, the algorithm optimizes N randomly sampled subproblems $g(\cdot; \boldsymbol{\alpha}^k)$, $k \in [N]$. For each subproblem, lines 4 to 6 sample λ random solutions from $\pi(\varphi_{\boldsymbol{\theta}}(\boldsymbol{\alpha}^k))$, and line 7 computes the gradient regarding this subproblem. Lines 4 to 7 cor-4 respond to an iteration of a typical ES algostithm. Line 8 estimates the gradient w.r.t. the 6 PSL problem in (4), which reads $\tilde{\nabla}\mathcal{J}(\boldsymbol{\theta}) = \mathbb{E}_{\boldsymbol{\alpha}\sim\mathcal{U}(\Delta_M)}[\tilde{\nabla}\bar{\mathcal{J}}_{\boldsymbol{\alpha}^k}(\boldsymbol{\theta})] \approx \frac{1}{N}\sum_{k=1}^N \tilde{\nabla}\bar{\mathcal{J}}_{\boldsymbol{\alpha}^k}(\boldsymbol{\theta}).^7$ Eventually, $\tilde{\nabla}\mathcal{J}(\boldsymbol{\theta})$ is back-propagated to $\boldsymbol{\theta}$, where $\boldsymbol{\eta}$ denotes the learning rate.

```
Algorithm 1: Neural-ES for black-box PSL
```

```
Input : A black-box MOP F(x)
Output: A set model \varphi_{\theta}
while The termination is not triggered do

for k = 1 to N do

Sample a preference \alpha^k \sim \mathcal{U}(\Delta_M),

set x_0 = \alpha^k;
for j = 1 to \lambda do

for i = 1 to p do

Construct x_i^j based on (8);

Compute \tilde{\nabla} \bar{\mathcal{J}}_{\alpha^k}(\theta) based on (11),

where f(\cdot) := -g(\cdot; \alpha^k);

\theta \leftarrow \theta + \frac{\eta}{N} \sum_{k=1}^{N} \tilde{\nabla} \bar{\mathcal{J}}_{\alpha^k}(\theta);
```

5 Experiments

5.1 Configurations

Black-Box Pareto Set Learning (BBO-PSL) suite To evaluate the performance of PSL algorithms, a test problem should meet a few fundamental requirements, including 1) closed-form PF and PS, 2) a complex shape of the PS manifold, 3) scalability to arbitrarily high dimensions, and 4) non-separability with a wide spectrum of the Hessian. However, most existing problem suites [43–46] either implement only a few of these requirements or include other interfering features that fall outside the scope of this paper. To this end, we present the novel BBO-PSL suite, which comprises eight instances (F1 to F8) and satisfies all the aforementioned requirements. Among them, F1 to F4 are bi-objective instances, and F5 to F8 are tri-objective.

Compared algorithms We compare Neural-ES 2 to the state-of-the-art and canonical EPSL [15], and configure Neural-ES by $d = \lfloor n/16 \rceil$, $N = \lfloor 5n/16 \rceil$, and $\lambda = 2 + \lfloor 1.5 \ln n \rceil$. Additionally, as MOEAs are widely recognized as one of the most effective methodologies for obtaining a set of non-dominated solutions, we consider two state-of-the-art MOEAs specifically designed for high-dimensional MOPs, namely LMO-CSO [34] and IM-MOEA/D [35]. Among the many MOEAs, LMO-CSO is favored for its superior handling of dimensional dependencies in complex and high-dimensional landscapes, while IM-MOEA/D makes a notable effort to elevate the canonical MOEA/D [8] to high dimensions by incorporating the popular inverse modeling technique [47]. Compared to most others, they are more lightweight with lower computational overhead, indicating better scalability to larger population sizes. Moreover, we synthesize an algorithm called EPSL-R1, by setting p = 1 in Neural-ES, which represents the simplest way to integrate PSL with an ES.

Metrics The Inverted Generational Distance (IGD) [48] is used as the performance metric, with a smaller value indicating better performance. Each algorithm is repeated 21 times on each BBO-PSL instance using different random seeds. For the three PSL algorithms, we evaluate their *testing performance*. To do so, we input a large number of preferences into a trained set model, which yields the same number of distributions; from each distribution, we randomly sample a solution, the collection of which form the *testing solution set*; finally, we measure the IGD value of the set and refer it as

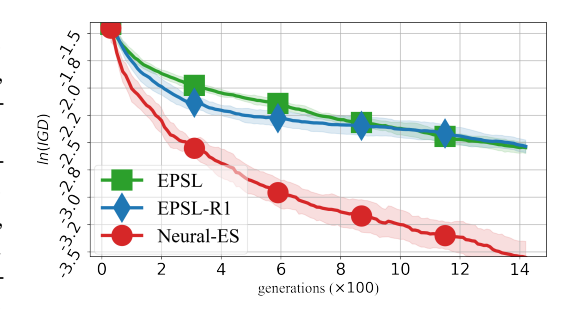


Figure 3: Convergence of the PSL algorithms on F1-128D.

the *testing IGD value*. Meanwhile, we track the convergence of the PSL algorithms during training, in terms of the IGD values acquired by the best solutions so far. The MOEAs directly optimize the

²The implementation of both Neural-ES and the BBO-PSL suite is available in https://github.com/chandler09/Neural-Evolution-Strategy.

same number of solutions, and the IGD value of the final population is measured. To examine the scalability of the algorithms with increasing dimensions, we vary n from 32 to 1024.

5.2 Results and discussions

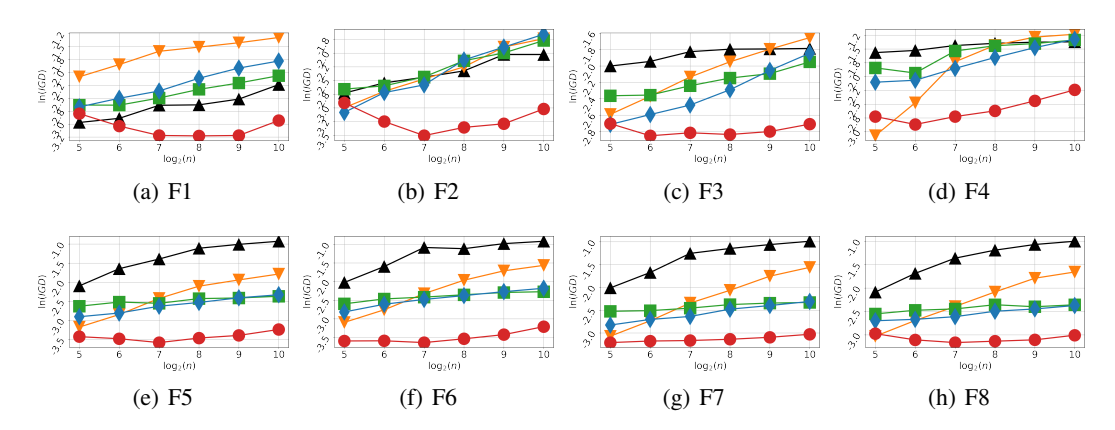


Figure 4: Average testing IGD values *w.r.t.* problem dimensions, where the red curve with circles refers to Neural-ES (ours), the blue curve with diamonds refers to EPSL-R1, the green curve with squares refers to EPSL, the orange curve with upside-down triangles refers to LMO-CSO, and finally the black curve with triangles refers to IM-MOEA/D. Their detailed values, along with the Mann-Whitney U test, can be found in Table 3.

According to Fig. 4, Neural-ES outperforms all the other algorithms in all eight instances by a large margin. Although the MOEAs are specialized for high-dimensional MOPs, they struggle to scale efficiently when users require numerous trade-offs among objectives. This drawback arises from their substantial demand on evaluation budgets and limited generalization ability. In contrast, the PSL paradigm performs well during surges in user demand, especially when demands shift or new ones emerge after optimization begins. The PSL algorithms, and Neural-ES in particular, are more robust against increasing problem dimensions. All these are attributed to the efficiency of evolution strategies and the generalization ability of the set model.

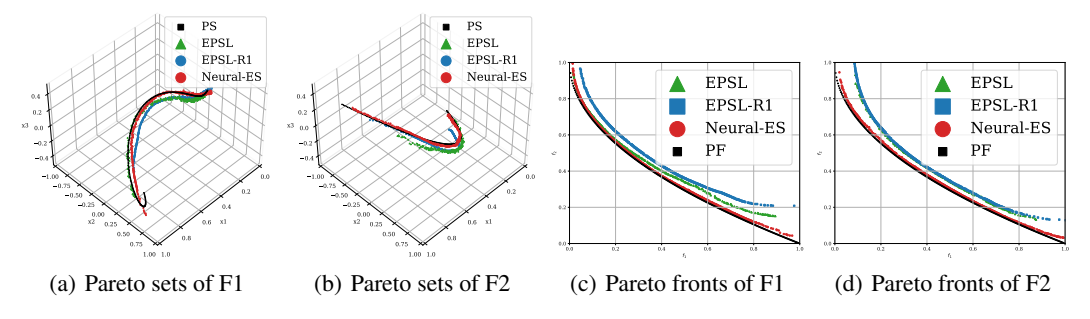


Figure 5: Testing solution sets of the algorithms, on F1-512D and F2-512D.

Compared to EPSL and EPSL-R1, Neural-ES reduces the IGD values by effectively decoupling the dimensional dependencies. Although EPSL-R1 also handles the dependencies, it performs slightly better than EPSL in just a few cases, yet remains similar overall. And its advantage over EPSL dissipates as n increases. This verifies that simply plugging an ES algorithm into adaptation-free scenarios, such as black-box PSL, does not yield a competitive algorithm. In contrast, the novel treatment of dimensional dependencies positions Neural-ES as a highly efficient alternative in adaptation-free scenarios.

In the remainder, we limit our focus to the PSL paradigm and utilize the limited space for in-depth discussions. In addition to the testing performance, we plot in Fig. 3 the training-time convergence of the three PSL algorithms. Neural-ES establishes a performance lead over EPSL and EPSL-R1

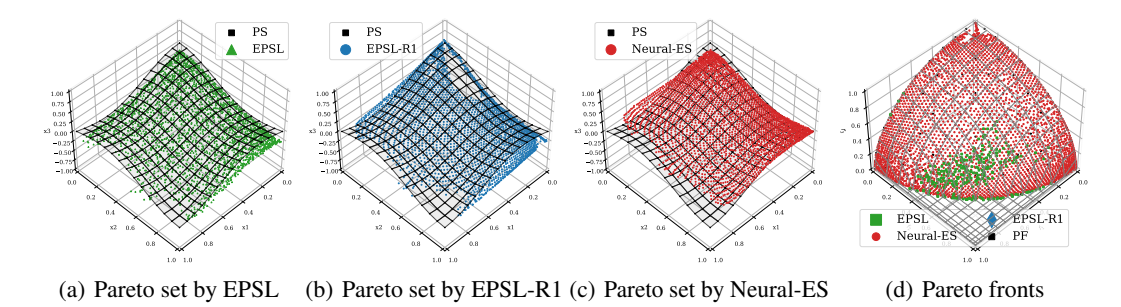


Figure 6: Testing solution sets of the algorithms, on F5-128D. For the ease of visualization, we only demonstrate the non-dominated solutions in 6(d). Therefore, the results of EPSL-R1 are unreported because none of its solutions are in $[0,1]^3$.

during the early stages, and subsequently extends the performance gap throughout the search process. The results suggest that Neural-ES efficiently learns the complex dimensional dependencies from the outset and exploits this advantage to significantly reduce the optimization difficulty.

The ability to approximate Pareto manifolds during testing is a unique feature of PSL as well as its primary priority. We plot in Figs. 5 and 6 some example approximation results. For the bi-objective F1 and F2, in Figs. 5(a) and 5(b), the approximate PSs by Neural-ES align more closely with the ground-truth and spread much wider than EPSL and EPSL-R1. It turns out that the approximate PFs by Neural-ES dominate those by the other two almost everywhere, as seen in Figs. 5(c) and 5(d).

Figs. 6(a) to 6(c) depict the approximate PSs in the first three dimensions of the search space (i.e., the $x_1-x_2-x_3$ subspace of the x-space). In these figures, the gray surface represents the ground-truth PS, while the colored points indicate the sampled solutions obtained by different algorithms during testing. In Fig. 6(a), solutions sampled by EPSL appear scattered and poorly aligned with preference vectors, because 1) the finite difference approach does not minimize the uncertainty of a distribution, and 2) EPSL does not learn the dimensional dependencies. Fig. 6(d) depicts the ground-truth PF (i.e., surface with gray contours) and the algorithm approximations in the objective space (i.e., the F-space), which provides a more rigorous performance assessment because it directly evaluates solution quality in the objective space and reveals dominance relationships that are not apparent in the x-space. While Neural-ES and EPSL-R1 appear similar in decision space (Figs. 6(a) to 6(c)), Neural-ES clearly outperforms in objective space, with most EPSL-R1 solutions being dominated by Neural-ES solutions.

5.3 Real-world applications

Trajectory planning We consider a tri-objective trajectory planning task modified from the popular rover problem [49, 33]. The goal is to determine a trajectory that minimizes 1) the cost during navigation, e.g., collisions with obstacles, 2) the distance from the endpoint to an intended target location, and 3) the total trajectory length, e.g., for saving energy. The objectives conflict with each other because, for instance, minimizing the distance may lead to increased frequency of collisions. We plan the trajectory by designing a total of 50 (x,y) coordinates, which means n = 100. Their approximate PFs are depicted in Fig. 7. Measured at a reference point of (5,2,1.5), Neural-ES, EPSL-R1, and EPSL achieve an average hypervolume of 8.314 ± 0.215 , 5.144 ± 0.622 , and 4.186 ± 0.709 , respectively, with higher values indicating better performance. Additionally, for each algorithm, we collect the optimal solutions for 300 evenly distributed subproblems. 299 out of 300 solutions from EPSL were dominated by those from Neural-ES, while 194 from EPSL-R1 were also dom-

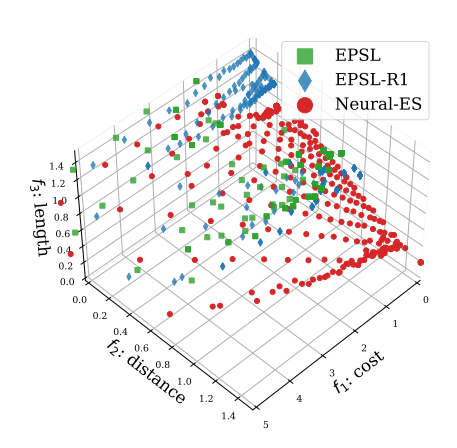


Figure 7: Approximate PFs of the trajectory planning problem.

inated by those from Neural-ES. The results demonstrate the superiority of Neural-ES in balancing the cost, distance, and total length of the trajectories.

Multi-objective Unmanned Aerial Vehicle (MO-UAV) Navigation We consider a set of real-world multi-objective MO-UAV navigation problems, which are featured in the Meta-BBO-v2 library [50] ³. This problem consists of three competing objectives: 1) the distance from the UAV's final location to the destination, penalized

Table 1: Average HV values and standard deviations, on the MO-UAV problems, with larger values the better.

Case	n	EPSL	EPSL-R1	Neural-ES
Easy	30	2.47 ± 0.36	1.58 ± 0.15	3.40 ± 0.28
Moderate	60	2.40 ± 0.37	1.52 ± 0.27	3.44 ± 0.45
Hard	120	0.72 ± 0.20	$0.84{\scriptstyle\pm0.14}$	2.44 ± 1.14

by the trajectory's non-smoothness, 2) the risk of collision with threats, such as ground-to-air missiles, and 3) an altitude penalty to maintain safe and cost-efficient flight. By varying the control parameters of the terrain, we have developed three instances: easy, moderate, and hard, which require a UAV trajectory of 10, 20, and 40 waypoints, respectively. Because each point comprises x, y, and z coordinates, the overall problem dimensions are 30, 60, and 120, respectively. Complex dimensional dependencies arise from the spatial and temporal correlations between waypoints, making navigation highly challenging. After 21 independent runs, we report the brief results in Table 1. Neural-ES demonstrates its superiority in practice with the highest HV values across all difficulty levels.

6 Conclusion, limitation, and future work

Conclusions In this work, we have made an initial effort to solve a novel yet important problem: black-box Pareto set learning (PSL). The goal is to learn the entire Pareto set of a black-box multi-objective function. We have developed a novel formulation, which facilitates the use of powerful black-box optimization algorithms, particularly evolution strategies. To address the challenges posed by black-box PSL, we have developed a novel mechanism to decouple the complex dimensional dependencies of the objectives. The proposed Neural-ES excels at learning challenging Pareto sets, successfully scaling the PSL paradigm to over 1000 dimensions with competitive performance.

Limitation and future work While this work focuses on unconstrained MOPs, constraints often significantly increase optimization difficulties, making constrained MOPs a critical area to address in PSL. Developing novel and advanced methods to extend PSL to constrained MOPs is a promising yet challenging direction for future research. Besides, Ye *et al.* [7] recently suggest that when reparameterizing an aggregation function $g(x;\alpha)$ as $\mathbb{E}_{\pi(x;\varphi)}[g(x;\alpha)]$, the optimization may only guarantee an approximate Pareto stationary point to be found, rather than an exact one, regardless of the specific distribution π . It is very interesting to further investigate what led to such a mismatch. Nonetheless, we believe that the formulation in (4) remains one of the best options available, and Ye *et al.* have also employed this reparameterization.

Acknowledgments

The work described in this paper was supported by the Research Grants Council of the Hong Kong Special Administrative Region, China [GRF Project No. CityU-11215723] and the Natural Science Foundation of China (Project No: 62276223). Zhenhua Li is supported in part by the Fundamental Research Funds for the Central Universities under No.NJ2024031.

³https://github.com/MetaEvo/MetaBox

References

- [1] K. M. Jablonka, G. M. Jothiappan, S. Wang, B. Smit, and B. Yoo, "Bias free multiobjective active learning for materials design and discovery," *Nature communications*, vol. 12, no. 1, p. 2312, 2021.
- [2] O. Sener and V. Koltun, "Multi-task learning as multi-objective optimization," *Advances in neural information processing systems*, vol. 31, 2018.
- [3] G. P. Rangaiah, Multi-objective optimization: techniques and applications in chemical engineering, vol. 5. world scientific, 2016.
- [4] K. Miettinen, Nonlinear multiobjective optimization, vol. 12. Springer Science & Business Media, 1999.
- [5] K. Li, "A survey of multi-objective evolutionary algorithm based on decomposition: Past and future," *IEEE Transactions on Evolutionary Computation*, 2024.
- [6] T. Huang, S. Wang, and K. Li, "Direct preference-based evolutionary multi-objective optimization with dueling bandits," Advances in Neural Information Processing Systems, vol. 37, pp. 122206–122258, 2024.
- [7] F. Ye, Y. Lyu, X. Wang, Y. Zhang, and I. Tsang, "Adaptive stochastic gradient algorithm for black-box multi-objective learning," in *The Twelfth International Conference on Learning Representations*, 2024.
- [8] Q. Zhang and H. Li, "MOEA/D: A multiobjective evolutionary algorithm based on decomposition," *IEEE Transactions on Evolutionary Computation*, vol. 11, no. 6, pp. 712–731, 2007.
- [9] X. Lin, Z. Yang, X. Zhang, and Q. Zhang, "Pareto set learning for expensive multi-objective optimization," in *Advances in neural information processing systems*, vol. 35, pp. 19231–19247, 2022.
- [10] E. Liu, Y.-C. Wu, X. Huang, C. Gao, R.-J. Wang, K. Xue, and C. Qian, "Pareto set learning for multiobjective reinforcement learning," in *Proceedings of the AAAI Conference on Artificial Intelligence*, 2025.
- [11] Y. Lu, B. Li, and A. Zhou, "Are you concerned about limited function evaluations: Data-augmented pareto set learning for expensive multi-objective optimization," in *Proceedings of the AAAI Conference on Artificial Intelligence*, pp. 14202–14210, 2024.
- [12] R. Ye, L. Chen, J. Zhang, and H. Ishibuchi, "Evolutionary preference sampling for pareto set learning," in *Proceedings of the Genetic and Evolutionary Computation Conference*, pp. 630–638, 2024.
- [13] M.-D. Nguyen, P. M. Dinh, Q.-H. Nguyen, L. P. Hoang, and D. D. Le, "Improving pareto set learning for expensive multi-objective optimization via stein variational hypernetworks," in *Proceedings of the AAAI Conference on Artificial Intelligence*, pp. 19677–19685, 2025.
- [14] Y. Liu, J. Yang, X. Ren, Z. Xinyi, Y. Liu, B. Song, X. Zeng, and H. Ishibuchi, "Multi-objective molecular design through learning latent pareto set," in *Proceedings of the AAAI Conference on Artificial Intelligence*, pp. 19006–19014, 2025.
- [15] X. Lin, X. Zhang, Z. Yang, and Q. Zhang, "Dealing with structure constraints in evolutionary pareto set learning," *IEEE Transactions on Evolutionary Computation*, 2025.
- [16] G. Lárraga and K. Miettinen, "Survey of interactive evolutionary decomposition-based multiobjective optimization methods," *Evolutionary Computation*, pp. 1–39, 2025.
- [17] Y. Shi, K. Xue, S. Lei, and C. Qian, "Macro placement by wire-mask-guided black-box optimization," *Advances in Neural Information Processing Systems*, vol. 36, pp. 6825–6843, 2023.
- [18] P. N. Williams and K. Li, "Black-box sparse adversarial attack via multi-objective optimisation," in Proceedings of the IEEE/CVF Conference on Computer Vision and Pattern Recognition, pp. 12291–12301, 2023.
- [19] N. Hansen and A. Ostermeier, "Completely derandomized self-adaptation in evolution strategies," *Evol. Comput.*, vol. 9, no. 2, pp. 159–195, 2001.
- [20] D. Wierstra, T. Schaul, T. Glasmachers, Y. Sun, J. Peters, and J. Schmidhuber, "Natural evolution strategies," The Journal of Machine Learning Research, vol. 15, no. 1, pp. 949–980, 2014.
- [21] R. T. Lange, T. Schaul, Y. Chen, T. Zahavy, V. Dalibard, C. Lu, S. Singh, and S. Flennerhag, "Discovering evolution strategies via meta-black-box optimization," in *The Eleventh International Conference on Learning Representations*, 2023.

- [22] O. Li, J. Harrison, J. Sohl-Dickstein, V. Smith, and L. Metz, "Variance-reduced gradient estimation via noise-reuse in online evolution strategies," *Advances in Neural Information Processing Systems*, vol. 36, pp. 45489–45501, 2023.
- [23] P. Vicol, L. Metz, and J. Sohl-Dickstein, "Unbiased gradient estimation in unrolled computation graphs with persistent evolution strategies," in *International Conference on Machine Learning*, pp. 10553–10563, PMLR, 2021.
- [24] N. Hansen, R. Ros, N. Mauny, M. Schoenauer, and A. Auger, "Impacts of invariance in search: When CMA-ES and PSO face ill-conditioned and non-separable problems," *Applied Soft Computing*, vol. 11, no. 8, pp. 5755–5769, 2011.
- [25] Y. Ollivier, L. Arnold, A. Auger, and N. Hansen, "Information-geometric optimization algorithms: A unifying picture via invariance principles," *Journal of Machine Learning Research*, vol. 18, no. 18, pp. 1–65, 2017.
- [26] H.-G. Beyer, "Convergence analysis of evolutionary algorithms that are based on the paradigm of information geometry," *Evolutionary Computation*, vol. 22, no. 4, pp. 679–709, 2014.
- [27] N. Hansen, S. D. Müller, and P. Koumoutsakos, "Reducing the time complexity of the derandomized evolution strategy with covariance matrix adaptation (CMA-ES)," *Evolutionary computation*, vol. 11, no. 1, pp. 1–18, 2003.
- [28] T. Glasmachers, T. Schaul, S. Yi, D. Wierstra, and J. Schmidhuber, "Exponential natural evolution strategies," in *Proceedings of the 12th annual conference on Genetic and evolutionary computation*, pp. 393–400, 2010.
- [29] Y. Akimoto, A. Auger, and N. Hansen, "Comparison-based natural gradient optimization in high dimension," in *Proceedings of the 2014 Annual Conference on Genetic and Evolutionary Computation*, pp. 373–380, 2014.
- [30] Z. Li and Q. Zhang, "A simple yet efficient evolution strategy for large-scale black-box optimization," IEEE Transactions on Evolutionary Computation, vol. 22, no. 5, pp. 637–646, 2017.
- [31] I. Loshchilov, T. Glasmachers, and H.-G. Beyer, "Large scale black-box optimization by limited-memory matrix adaptation," *IEEE Transactions on Evolutionary Computation*, vol. 23, no. 2, pp. 353–358, 2018.
- [32] J. Martens, "New insights and perspectives on the natural gradient method," *Journal of Machine Learning Research*, vol. 21, no. 146, pp. 1–76, 2020.
- [33] S. Daulton, D. Eriksson, M. Balandat, and E. Bakshy, "Multi-objective bayesian optimization over high-dimensional search spaces," in *Uncertainty in Artificial Intelligence*, pp. 507–517, PMLR, 2022.
- [34] Y. Tian, X. Zheng, X. Zhang, and Y. Jin, "Efficient large-scale multiobjective optimization based on a competitive swarm optimizer," *IEEE Transactions on Cybernetics*, vol. 50, no. 8, pp. 3696–3708, 2020.
- [35] L. R. Farias and A. F. Araújo, "Im-moea/d: An inverse modeling multi-objective evolutionary algorithm based on decomposition," in 2021 ieee international conference on systems, man, and cybernetics (SMC), pp. 462–467, IEEE, 2021.
- [36] X. Lin, Z. Yang, and Q. Zhang, "Pareto set learning for neural multi-objective combinatorial optimization," in *International Conference on Learning Representation*, 2022.
- [37] X. Zhang, X. Lin, B. Xue, Y. Chen, and Q. Zhang, "Hypervolume maximization: A geometric view of pareto set learning," Advances in Neural Information Processing Systems, vol. 36, pp. 38902–38929, 2023.
- [38] H.-G. Beyer and B. Sendhoff, "Simplify your covariance matrix adaptation evolution strategy," *IEEE Transactions on Evolutionary Computation*, vol. 21, no. 5, pp. 746–759, 2017.
- [39] Y. Akimoto, Y. Nagata, I. Ono, and S. Kobayashi, "Bidirectional relation between cma evolution strategies and natural evolution strategies," in *Parallel Problem Solving from Nature*, PPSN XI: 11th International Conference, Kraków, Poland, September 11-15, 2010, Proceedings, Part I 11, pp. 154–163, Springer, 2010.
- [40] N. Hansen and A. Auger, "Principled design of continuous stochastic search: From theory to practice," in *Theory and principled methods for the design of metaheuristics*, pp. 145–180, Springer, 2013.
- [41] R. Hamano, S. Shirakawa, and M. Nomura, "Natural gradient interpretation of rank-one update in CMA-ES," in *International Conference on Parallel Problem Solving from Nature*, pp. 252–267, Springer, 2024.

- [42] Y. Sun, T. Schaul, F. Gomez, and J. Schmidhuber, "A linear time natural evolution strategy for non-separable functions," in *Proceedings of the 15th annual conference companion on Genetic and evolutionary computation*, pp. 61–62, 2013.
- [43] Q. Zhang, A. Zhou, S. Zhao, P. N. Suganthan, W. Liu, S. Tiwari, *et al.*, "Multiobjective optimization test instances for the cec 2009 special session and competition," tech. rep., Colchester, UK, 2008.
- [44] D. Brockhoff, A. Auger, N. Hansen, and T. Tušar, "Using well-understood single-objective functions in multiobjective black-box optimization test suites," *Evolutionary Computation*, vol. 30, no. 2, pp. 165–193, 2022.
- [45] R. Cheng, Y. Jin, M. Olhofer, et al., "Test problems for large-scale multiobjective and many-objective optimization," *IEEE transactions on cybernetics*, vol. 47, no. 12, pp. 4108–4121, 2016.
- [46] S. Zapotecas-Martínez, C. A. C. Coello, H. E. Aguirre, and K. Tanaka, "Challenging test problems for multi-and many-objective optimization," Swarm and Evolutionary Computation, vol. 81, p. 101350, 2023.
- [47] R. Cheng, Y. Jin, K. Narukawa, and B. Sendhoff, "A multiobjective evolutionary algorithm using gaussian process-based inverse modeling," *IEEE Transactions on Evolutionary Computation*, vol. 19, no. 6, pp. 838– 856, 2015.
- [48] J. G. Falcón-Cardona and C. A. C. Coello, "Indicator-based multi-objective evolutionary algorithms: A comprehensive survey," ACM Computing Surveys (CSUR), vol. 53, no. 2, pp. 1–35, 2020.
- [49] Z. Wang, C. Gehring, P. Kohli, and S. Jegelka, "Batched large-scale bayesian optimization in high-dimensional spaces," in *International Conference on Artificial Intelligence and Statistics*, pp. 745–754, PMLR, 2018.
- [50] Z. Ma, Y.-J. Gong, H. Guo, W. Qiu, S. Ma, H. Lian, J. Zhan, K. Chen, C. Wang, Z. Huang, et al., "Metabox-v2: A unified benchmark platform for meta-black-box optimization," arXiv preprint arXiv:2505.17745, 2025.
- [51] K. Gao and O. Sener, "Generalizing gaussian smoothing for random search," in *International Conference on Machine Learning*, pp. 7077–7101, PMLR, 2022.
- [52] K. Choromanski, M. Rowland, V. Sindhwani, R. Turner, and A. Weller, "Structured evolution with compact architectures for scalable policy optimization," in *International Conference on Machine Learning*, pp. 970–978, PMLR, 2018.
- [53] S. P. Boyd and L. Vandenberghe, Convex optimization. Cambridge university press, 2004.
- [54] S. Yi, D. Wierstra, T. Schaul, and J. Schmidhuber, "Stochastic search using the natural gradient," in *Proceedings of the 26th annual international conference on machine learning*, pp. 1161–1168, 2009.
- [55] Z. Li and Q. Zhang, "What does the evolution path learn in cma-es?," in *International Conference on Parallel Problem Solving from Nature*, pp. 751–760, Springer, 2016.
- [56] Y. Akimoto and N. Hansen, "Diagonal acceleration for covariance matrix adaptation evolution strategies," Evolutionary computation, vol. 28, no. 3, pp. 405–435, 2020.
- [57] Y. Akimoto and N. Hansen, "Projection-based restricted covariance matrix adaptation for high dimension," in *Proceedings of the Genetic and Evolutionary Computation Conference 2016*, pp. 197–204, 2016.
- [58] Y. Lyu and I. W. Tsang, "Black-box optimizer with stochastic implicit natural gradient," in *Joint European conference on machine learning and knowledge discovery in databases*, pp. 217–232, Springer, 2021.
- [59] Y. Lyu, "Fast rank-1 lattice targeted sampling for black-box optimization," Advances in Neural Information Processing Systems, vol. 36, pp. 10494–10515, 2023.
- [60] B. Li, J. Li, K. Tang, and X. Yao, "Many-objective evolutionary algorithms: A survey," ACM Computing Surveys (CSUR), vol. 48, no. 1, pp. 1–35, 2015.
- [61] D. A. Harville, "Matrix algebra from a statistician's perspective," 1998.
- [62] S.-I. Amari, "Natural gradient works efficiently in learning," *Neural computation*, vol. 10, no. 2, pp. 251–276, 1998.
- [63] K. Deb, L. Thiele, M. Laumanns, and E. Zitzler, "Scalable test problems for evolutionary multiobjective optimization," in *Evolutionary multiobjective optimization: theoretical advances and applications*, pp. 105– 145, Springer, 2005.

- [64] H. Li and Q. Zhang, "Multiobjective optimization problems with complicated pareto sets, moea/d and nsga-ii," *IEEE transactions on evolutionary computation*, vol. 13, no. 2, pp. 284–302, 2008.
- [65] Y. Tian, R. Cheng, X. Zhang, and Y. Jin, "PlatEMO: A MATLAB platform for evolutionary multi-objective optimization," *IEEE Computational Intelligence Magazine*, vol. 12, no. 4, pp. 73–87, 2017.

NeurIPS Paper Checklist

1. Claims

Question: Do the main claims made in the abstract and introduction accurately reflect the paper's contributions and scope?

Answer: [Yes]

Justification: The abstract and introduction clearly state the claims, including the contributions made and limitations. We carefully exclude any over-claim of our contributions.

Guidelines:

- The answer NA means that the abstract and introduction do not include the claims made in the paper.
- The abstract and/or introduction should clearly state the claims made, including the contributions
 made in the paper and important assumptions and limitations. A No or NA answer to this
 question will not be perceived well by the reviewers.
- The claims made should match theoretical and experimental results, and reflect how much the results can be expected to generalize to other settings.
- It is fine to include aspirational goals as motivation as long as it is clear that these goals are not attained by the paper.

2. Limitations

Question: Does the paper discuss the limitations of the work performed by the authors?

Answer: [Yes]

This paper discusses constrained multiobjective optimization problems, a prevalent area that remains unsolved.

Guidelines:

- The answer NA means that the paper has no limitation while the answer No means that the paper has limitations, but those are not discussed in the paper.
- The authors are encouraged to create a separate "Limitations" section in their paper.
- The paper should point out any strong assumptions and how robust the results are to violations of these assumptions (e.g., independence assumptions, noiseless settings, model well-specification, asymptotic approximations only holding locally). The authors should reflect on how these assumptions might be violated in practice and what the implications would be.
- The authors should reflect on the scope of the claims made, e.g., if the approach was only tested
 on a few datasets or with a few runs. In general, empirical results often depend on implicit
 assumptions, which should be articulated.
- The authors should reflect on the factors that influence the performance of the approach. For example, a facial recognition algorithm may perform poorly when image resolution is low or images are taken in low lighting. Or a speech-to-text system might not be used reliably to provide closed captions for online lectures because it fails to handle technical jargon.
- The authors should discuss the computational efficiency of the proposed algorithms and how
 they scale with dataset size.
- If applicable, the authors should discuss possible limitations of their approach to address problems
 of privacy and fairness.
- While the authors might fear that complete honesty about limitations might be used by reviewers
 as grounds for rejection, a worse outcome might be that reviewers discover limitations that
 aren't acknowledged in the paper. The authors should use their best judgment and recognize
 that individual actions in favor of transparency play an important role in developing norms that
 preserve the integrity of the community. Reviewers will be specifically instructed to not penalize
 honesty concerning limitations.

3. Theory assumptions and proofs

Question: For each theoretical result, does the paper provide the full set of assumptions and a complete (and correct) proof?

Answer: [Yes]

We provide detailed proofs and derivations in the supplementary materials. All theorems, formulas, and proofs in the paper are numbered and cross-referenced. All assumptions are clearly stated or referenced in the statement of any theorems.

Guidelines:

• The answer NA means that the paper does not include theoretical results.

- All the theorems, formulas, and proofs in the paper should be numbered and cross-referenced.
- All assumptions should be clearly stated or referenced in the statement of any theorems.
- The proofs can either appear in the main paper or the supplemental material, but if they appear in the supplemental material, the authors are encouraged to provide a short proof sketch to provide intuition.
- Inversely, any informal proof provided in the core of the paper should be complemented by formal proofs provided in appendix or supplemental material.
- Theorems and Lemmas that the proof relies upon should be properly referenced.

4. Experimental result reproducibility

Question: Does the paper fully disclose all the information needed to reproduce the main experimental results of the paper to the extent that it affects the main claims and/or conclusions of the paper (regardless of whether the code and data are provided or not)?

Answer: [Yes]

Justification: The steps of our proposed algorithms are described step by step. The code will be open-sourced upon article acceptance for reproducibility of experiments.

Guidelines:

- The answer NA means that the paper does not include experiments.
- If the paper includes experiments, a No answer to this question will not be perceived well by the reviewers: Making the paper reproducible is important, regardless of whether the code and data are provided or not.
- If the contribution is a dataset and/or model, the authors should describe the steps taken to make their results reproducible or verifiable.
- Depending on the contribution, reproducibility can be accomplished in various ways. For example, if the contribution is a novel architecture, describing the architecture fully might suffice, or if the contribution is a specific model and empirical evaluation, it may be necessary to either make it possible for others to replicate the model with the same dataset, or provide access to the model. In general, releasing code and data is often one good way to accomplish this, but reproducibility can also be provided via detailed instructions for how to replicate the results, access to a hosted model (e.g., in the case of a large language model), releasing of a model checkpoint, or other means that are appropriate to the research performed.
- While NeurIPS does not require releasing code, the conference does require all submissions
 to provide some reasonable avenue for reproducibility, which may depend on the nature of the
 contribution. For example
 - (a) If the contribution is primarily a new algorithm, the paper should make it clear how to reproduce that algorithm.
 - (b) If the contribution is primarily a new model architecture, the paper should describe the architecture clearly and fully.
 - (c) If the contribution is a new model (e.g., a large language model), then there should either be a way to access this model for reproducing the results or a way to reproduce the model (e.g., with an open-source dataset or instructions for how to construct the dataset).
 - (d) We recognize that reproducibility may be tricky in some cases, in which case authors are welcome to describe the particular way they provide for reproducibility. In the case of closed-source models, it may be that access to the model is limited in some way (e.g., to registered users), but it should be possible for other researchers to have some path to reproducing or verifying the results.

5. Open access to data and code

Question: Does the paper provide open access to the data and code, with sufficient instructions to faithfully reproduce the main experimental results, as described in supplemental material?

Answer: [Yes]

Justification: The code will be open-sourced upon article acceptance.

Guidelines:

- The answer NA means that paper does not include experiments requiring code.
- Please see the NeurIPS code and data submission guidelines (https://nips.cc/public/guides/CodeSubmissionPolicy) for more details.
- While we encourage the release of code and data, we understand that this might not be possible, so "No" is an acceptable answer. Papers cannot be rejected simply for not including code, unless this is central to the contribution (e.g., for a new open-source benchmark).

- The instructions should contain the exact command and environment needed to run to reproduce
 the results. See the NeurIPS code and data submission guidelines (https://nips.cc/public/
 guides/CodeSubmissionPolicy) for more details.
- The authors should provide instructions on data access and preparation, including how to access the raw data, preprocessed data, intermediate data, and generated data, etc.
- The authors should provide scripts to reproduce all experimental results for the new proposed method and baselines. If only a subset of experiments are reproducible, they should state which ones are omitted from the script and why.
- At submission time, to preserve anonymity, the authors should release anonymized versions (if applicable).
- Providing as much information as possible in supplemental material (appended to the paper) is recommended, but including URLs to data and code is permitted.

6. Experimental setting/details

Question: Does the paper specify all the training and test details (e.g., data splits, hyperparameters, how they were chosen, type of optimizer, etc.) necessary to understand the results?

Answer: [Yes]

Justification: The vital experimental settings are presented in the core of the paper, Section 5. And the full details can be referenced in the supplementary document.

Guidelines

- The answer NA means that the paper does not include experiments.
- The experimental setting should be presented in the core of the paper to a level of detail that is necessary to appreciate the results and make sense of them.
- The full details can be provided either with the code, in appendix, or as supplemental material.

7. Experiment statistical significance

Question: Does the paper report error bars suitably and correctly defined or other appropriate information about the statistical significance of the experiments?

Answer: [Yes]

Justification: The experiment results are accompanied by statistical significance tests, i.e., the Mann-Whitney U test.

Guidelines:

- The answer NA means that the paper does not include experiments.
- The authors should answer "Yes" if the results are accompanied by error bars, confidence intervals, or statistical significance tests, at least for the experiments that support the main claims of the paper.
- The factors of variability that the error bars are capturing should be clearly stated (for example, train/test split, initialization, random drawing of some parameter, or overall run with given experimental conditions).
- The method for calculating the error bars should be explained (closed form formula, call to a library function, bootstrap, etc.)
- $\bullet\,$ The assumptions made should be given (e.g., Normally distributed errors).
- It should be clear whether the error bar is the standard deviation or the standard error of the mean
- It is OK to report 1-sigma error bars, but one should state it. The authors should preferably report
 a 2-sigma error bar than state that they have a 96% CI, if the hypothesis of Normality of errors is
 not verified.
- For asymmetric distributions, the authors should be careful not to show in tables or figures symmetric error bars that would yield results that are out of range (e.g. negative error rates).
- If error bars are reported in tables or plots, The authors should explain in the text how they were calculated and reference the corresponding figures or tables in the text.

8. Experiments compute resources

Question: For each experiment, does the paper provide sufficient information on the computer resources (type of compute workers, memory, time of execution) needed to reproduce the experiments?

Answer: [Yes

Justification: We record the information on the computer resources in the supplementary document. Guidelines:

- The answer NA means that the paper does not include experiments.
- The paper should indicate the type of compute workers CPU or GPU, internal cluster, or cloud provider, including relevant memory and storage.
- The paper should provide the amount of compute required for each of the individual experimental runs as well as estimate the total compute.
- The paper should disclose whether the full research project required more compute than the experiments reported in the paper (e.g., preliminary or failed experiments that didn't make it into the paper).

9. Code of ethics

Question: Does the research conducted in the paper conform, in every respect, with the NeurIPS Code of Ethics https://neurips.cc/public/EthicsGuidelines?

Answer: [Yes

Justification: The authors make sure to preserve anonymity.

Guidelines:

- The answer NA means that the authors have not reviewed the NeurIPS Code of Ethics.
- If the authors answer No, they should explain the special circumstances that require a deviation from the Code of Ethics.
- The authors should make sure to preserve anonymity (e.g., if there is a special consideration due to laws or regulations in their jurisdiction).

10. Broader impacts

Question: Does the paper discuss both potential positive societal impacts and negative societal impacts of the work performed?

Answer: [NA]

Justification: This paper is foundational research and not tied to particular applications, let alone deployments.

Guidelines:

- The answer NA means that there is no societal impact of the work performed.
- If the authors answer NA or No, they should explain why their work has no societal impact or why the paper does not address societal impact.
- Examples of negative societal impacts include potential malicious or unintended uses (e.g., disinformation, generating fake profiles, surveillance), fairness considerations (e.g., deployment of technologies that could make decisions that unfairly impact specific groups), privacy considerations, and security considerations.
- The conference expects that many papers will be foundational research and not tied to particular applications, let alone deployments. However, if there is a direct path to any negative applications, the authors should point it out. For example, it is legitimate to point out that an improvement in the quality of generative models could be used to generate deepfakes for disinformation. On the other hand, it is not needed to point out that a generic algorithm for optimizing neural networks could enable people to train models that generate Deepfakes faster.
- The authors should consider possible harms that could arise when the technology is being used
 as intended and functioning correctly, harms that could arise when the technology is being used
 as intended but gives incorrect results, and harms following from (intentional or unintentional)
 misuse of the technology.
- If there are negative societal impacts, the authors could also discuss possible mitigation strategies
 (e.g., gated release of models, providing defenses in addition to attacks, mechanisms for monitoring misuse, mechanisms to monitor how a system learns from feedback over time, improving the
 efficiency and accessibility of ML).

11. Safeguards

Question: Does the paper describe safeguards that have been put in place for responsible release of data or models that have a high risk for misuse (e.g., pretrained language models, image generators, or scraped datasets)?

Answer: [NA]

Justification: This paper poses no such risks

Guidelines:

The answer NA means that the paper poses no such risks.

- Released models that have a high risk for misuse or dual-use should be released with necessary safeguards to allow for controlled use of the model, for example by requiring that users adhere to usage guidelines or restrictions to access the model or implementing safety filters.
- Datasets that have been scraped from the Internet could pose safety risks. The authors should describe how they avoided releasing unsafe images.
- We recognize that providing effective safeguards is challenging, and many papers do not require
 this, but we encourage authors to take this into account and make a best faith effort.

12. Licenses for existing assets

Question: Are the creators or original owners of assets (e.g., code, data, models), used in the paper, properly credited and are the license and terms of use explicitly mentioned and properly respected?

Answer: [NA]

Justification: The creators or original owners of assets (e.g., code, data, models), used in the paper, are properly credited and are the license and terms of use explicitly mentioned and properly respected.

Guidelines:

- The answer NA means that the paper does not use existing assets.
- The authors should cite the original paper that produced the code package or dataset.
- The authors should state which version of the asset is used and, if possible, include a URL.
- The name of the license (e.g., CC-BY 4.0) should be included for each asset.
- For scraped data from a particular source (e.g., website), the copyright and terms of service of that source should be provided.
- If assets are released, the license, copyright information, and terms of use in the package should be provided. For popular datasets, paperswithcode.com/datasets has curated licenses for some datasets. Their licensing guide can help determine the license of a dataset.
- For existing datasets that are re-packaged, both the original license and the license of the derived asset (if it has changed) should be provided.
- If this information is not available online, the authors are encouraged to reach out to the asset's
 creators.

13. New assets

Question: Are new assets introduced in the paper well documented and is the documentation provided alongside the assets?

Answer: [NA]

Justification: This paper does not release new assets

Guidelines:

- The answer NA means that the paper does not release new assets.
- Researchers should communicate the details of the dataset/code/model as part of their submissions via structured templates. This includes details about training, license, limitations, etc.
- The paper should discuss whether and how consent was obtained from people whose asset is used.
- At submission time, remember to anonymize your assets (if applicable). You can either create an
 anonymized URL or include an anonymized zip file.

14. Crowdsourcing and research with human subjects

Question: For crowdsourcing experiments and research with human subjects, does the paper include the full text of instructions given to participants and screenshots, if applicable, as well as details about compensation (if any)?

Answer: [NA]

Justification: The paper does not involve crowdsourcing nor research with human subjects

Guidelines:

- The answer NA means that the paper does not involve crowdsourcing nor research with human subjects.
- Including this information in the supplemental material is fine, but if the main contribution of the
 paper involves human subjects, then as much detail as possible should be included in the main
 paper.
- According to the NeurIPS Code of Ethics, workers involved in data collection, curation, or other labor should be paid at least the minimum wage in the country of the data collector.

15. Institutional review board (IRB) approvals or equivalent for research with human subjects

Question: Does the paper describe potential risks incurred by study participants, whether such risks were disclosed to the subjects, and whether Institutional Review Board (IRB) approvals (or an equivalent approval/review based on the requirements of your country or institution) were obtained?

Answer: [NA]

Justification: The paper does not involve crowdsourcing nor research with human subjects.

Guidelines:

- The answer NA means that the paper does not involve crowdsourcing nor research with human subjects.
- Depending on the country in which research is conducted, IRB approval (or equivalent) may be required for any human subjects research. If you obtained IRB approval, you should clearly state this in the paper.
- We recognize that the procedures for this may vary significantly between institutions and locations, and we expect authors to adhere to the NeurIPS Code of Ethics and the guidelines for their institution.
- For initial submissions, do not include any information that would break anonymity (if applicable), such as the institution conducting the review.

16. Declaration of LLM usage

Question: Does the paper describe the usage of LLMs if it is an important, original, or non-standard component of the core methods in this research? Note that if the LLM is used only for writing, editing, or formatting purposes and does not impact the core methodology, scientific rigorousness, or originality of the research, declaration is not required.

Answer: [NA]

Justification: LLM is not involved other than writing, editing, or formatting purposes of this paper. Guidelines:

- The answer NA means that the core method development in this research does not involve LLMs
 as any important, original, or non-standard components.
- Please refer to our LLM policy (https://neurips.cc/Conferences/2025/LLM) for what should or should not be described.

A Additional related works

A.1 Evolution strategies

ES [20, 25, 21] is a prominent class of second-order black-box optimization methods. Compared to zeroth-order methods that leverage probability distribution models in their simplest forms and usually amount to finite-difference approaches [51, 52], ES is considered second-order because they are closely related to the quasi-Newton method [53]: they typically learn a covariance matrix that converges to the inverse of the objective's Hessian.

Wierstra *et al.* [20] proposed the Natural Evolution Strategy (NES), which amounts to a stochastic natural gradient ascent. Since its publication, several NES variants have emerged [54, 28, 42], addressing the issue with the Fisher information matrix using different parameterization strategies. Both Akimoto *et al.* [39] and Glasmachers *et al.* [28] derived the rank- μ update of CMA-ES from natural gradient, bridging gradient search and state-of-the-art ES. The primary difference between CMA-ES and NES, which makes the former superior, is that CMA-ES leverages two evolution paths that act as the momentum term in gradient search [55], one for updating the covariance matrix, while the other for tuning the isotropic mutation strength.

The covariance matrix of the Gaussian distribution is one of the most contributing parameters of ES. Through extensive experiments, Hansen *et al.* [24] showed that with the help of an adaptive covariance matrix, CMA-ES is not affected by coordinate system rotations, and is more resistant to the increase of the condition number. Beyer [26] proved that the covariance matrix gets asymptotically proportional to the inverse of the objective's Hessian, which is preferable as it counteracts the degeneration tendencies of the search distribution into a subspace.

The $\Theta(n^2)$ space and time complexities regarding the covariance matrix hinder the application of ES to large-scale problems. Several methods have been proposed to remedy the issue. These methods agree on simplifying the covariance matrix, while differing in the details of designing and updating the matrix. Sun *et al.* [42] proposed R1-NES, where a rank-one model is adopted as the covariance matrix, and the update is completely derived from natural gradient ascent. Akimoto *et al.* [29] proposed VD-CMA, where the covariance matrix is parameterized by the multiplication of a rank-one model, and a diagonal matrix that captures the scaling of each dimension. They derived the update from natural gradient and, in the meantime, incorporated the cumulation techniques of evolution paths from CMA-ES. The experiments demonstrated that VD-CMA significantly outperformed R1-NES. The multiplicative model in VD-CMA is further pursued in dd-CMA [56], a recent method that can well adapt to both separable and non-separable scenarios. A straightforward extension to the rank-one model is to apply more than one component to capture multiple promising search directions simultaneously, which yields much more efficient algorithms [57, 30, 31].

Although some recently proposed ESs are versatile across various tasks [23, 22], it may be more appropriate to classify them as zeroth-order methods, considering that they mainly focus on reducing the variance of the finite difference without utilizing second-order information. On the other hand, while some other methods do not explicitly identify as ESs [58, 59], they are to some extent inspired by ESs and share many common principles. Notably, Lyu and Tsang [58] proposed a black-box optimization algorithm called Implicit Natural Gradient Optimization (INGO). To avoid explicitly inverting the Fisher, they formulated a surrogate objective where the KL-divergence is attached as a penalty term and can be explicitly derived. The authors showed that the gradient with respect to the expectation of the sufficient statistics amounts to the natural gradient of the natural parameter of an exponential-family distribution. Since the Hessian of an objective primarily characterizes the dimensional dependencies, we focus exclusively on second-order methods.

A.2 Black-box multi-objective optimization

Multi-objective optimization (MOO) has consistently garnered significant attention [33, 7, 33]. In black-box MOO, multi-objective evolutionary algorithms (MOEAs) remain among the most dominant methodologies [6, 8, 60]. This is because MOEAs excel in maintaining a large population of solutions, and can thus approach the underlying Pareto Front (PF) from all directions. Recently, dedicated efforts have been made to extend MOEAs to high-dimensional, or in other words, large-scale MOPs. For instance, IM-MOEA/D [35] integrates the canonical MOEA/D [5] with an inverse model [47] which directly samples in the objective space using Gaussian process models, and then maps into the decision space. Focusing on the complex landscapes in high-dimensional MOPs, LMO-CSO [34] proposes addressing the dimensional dependencies using an efficient particle swarm optimization (PSO) algorithm. Among the three mainstream MOEAs, those based on Pareto dominance and performance indicators fall short of aligning with decision-makers' preferences and scale poorly with the number of solutions [60], due to the high computational overhead associated with non-dominated sorting and hypervolume contribution. Meanwhile, decomposition-based MOEAs [5] struggle with only a limited number of pre-established preferences, generalize poorly to the entire Pareto manifold, and encounter difficulties in sharing information across subproblems.

B More details about Neural-ES

This section is arranged as follows:

- Section B.1 shows that random samples generated by (8) are in-distribution of $\pi(\cdot; \varphi)$, where $\varphi = \varphi_{\theta}(\alpha)$;
- Section B.2 provides derivation for the vanilla gradient $\nabla \bar{\mathcal{J}}_{\alpha}(\theta)$ in (9), and analyzes its major drawback, that is, it potentially leads to divergent behaviors of the search distribution.
- Section B.3 justifies the use of the Fisher from the perspective of natural gradient, and derives (10).
- Section B.4 further transforms the gradient (10) to the practical update rule (11) used in the algorithm.
- Sections B.5 and B.6 provide more details on the weight values and the set model.
- Section B.7 derives the space and time complexity of Neural-ES, demonstrating its time efficiency.

B.1 Proof of Equation (8)

Proposition 1. A solution generated by (8) follows the distribution $\pi(\cdot; \varphi)$, where $\varphi = \varphi_{\theta}(\alpha)$.

Proof. Consider the solution $\boldsymbol{x}=(\boldsymbol{x}_1,...,\boldsymbol{x}_p)$ where $\boldsymbol{x}_i=\boldsymbol{m}_{\boldsymbol{\theta}}(\boldsymbol{x}_{0:i-1})+\sigma_{\boldsymbol{\theta}}(\boldsymbol{x}_{0:i-1})(\boldsymbol{z}+r\boldsymbol{v}_{\boldsymbol{\theta}}(\boldsymbol{x}_{0:i-1}))$ for all $i\in[p], \boldsymbol{z}\sim\mathcal{N}(\boldsymbol{0},\boldsymbol{I})$, and $r\sim\mathcal{N}(0,1)$. To prove $\boldsymbol{x}\sim\pi(\boldsymbol{\varphi})$ is equivalent to proving that $(\boldsymbol{x}_1,...,\boldsymbol{x}_p)$ follows the joint distribution $\prod_{i=1}^p\mathcal{N}_{\boldsymbol{\theta}}(\cdot|\boldsymbol{x}_0,\boldsymbol{x}_1,...,\boldsymbol{x}_{i-1})$ where $\boldsymbol{x}_0=\boldsymbol{\alpha}$.

Note that for an arbitrary $i \in [p]$, the expectation of x_i is given by:

$$\mathbb{E}[oldsymbol{x}_i] = oldsymbol{m}_{oldsymbol{ heta}}(oldsymbol{x}_{0:i-1}) + \sigma_{oldsymbol{ heta}}(oldsymbol{x}_{0:i-1}) \left(\underbrace{\mathbb{E}[oldsymbol{z}]}_{=oldsymbol{ heta}} + \underbrace{\mathbb{E}[r]}_{=oldsymbol{ heta}} oldsymbol{v}_{oldsymbol{ heta}}(oldsymbol{x}_{0:i-1})
ight) = oldsymbol{m}_{oldsymbol{ heta}}(oldsymbol{x}_{0:i-1}),$$

and the covariance matrix is given by:

$$\begin{split} &\mathbb{E}\left[(\boldsymbol{x}_i - \boldsymbol{m}_{\boldsymbol{\theta}}(\boldsymbol{x}_{0:i-1}))(\boldsymbol{x}_i - \boldsymbol{m}_{\boldsymbol{\theta}}(\boldsymbol{x}_{0:i-1}))^T\right] \\ &= \sigma_{\boldsymbol{\theta}}(\boldsymbol{x}_{0:i-1})^2 \left(\underbrace{\mathbb{E}[\boldsymbol{z}\boldsymbol{z}^T]}_{=\boldsymbol{I}} + \boldsymbol{v}_{\boldsymbol{\theta}}(\boldsymbol{x}_{0:i-1})\mathbb{E}[r\boldsymbol{z}]^T + \mathbb{E}[r\boldsymbol{z}]\boldsymbol{v}_{\boldsymbol{\theta}}(\boldsymbol{x}_{0:i-1})^T + \underbrace{\mathbb{E}[r^2]}_{=\boldsymbol{I}}\boldsymbol{v}_{\boldsymbol{\theta}}(\boldsymbol{x}_{0:i-1})\boldsymbol{v}_{\boldsymbol{\theta}}(\boldsymbol{x}_{0:i-1})^T\right) \\ &= \sigma_{\boldsymbol{\theta}}(\boldsymbol{x}_{0:i-1})^2 \left(\boldsymbol{I} + \boldsymbol{v}_{\boldsymbol{\theta}}(\boldsymbol{x}_{0:i-1})\boldsymbol{v}_{\boldsymbol{\theta}}(\boldsymbol{x}_{0:i-1})^T\right) = \boldsymbol{C}_{\boldsymbol{\theta}}(\boldsymbol{x}_{0:i-1}), \end{split}$$

which is because $\mathbb{E}[rz] = \mathbb{E}[r]\mathbb{E}[z] = \mathbf{0}$, as r and z are independent from each other. Therefore, for all $i \in [p]$, $x_i \sim \mathcal{N}(m_{\theta}(x_{0:i-1}), C_{\theta}(x_{0:i-1}))$, and $\mathcal{N}(m_{\theta}(x_{0:i-1}), C_{\theta}(x_{0:i-1})) = \mathcal{N}_{\theta}(\cdot|x_0, x_1, ..., x_{i-1})$.

By the definition of joint distribution, we have:

$$egin{aligned} & (oldsymbol{x}_1, oldsymbol{x}_2) \sim \mathcal{N}_{oldsymbol{ heta}}(\cdot | oldsymbol{x}_0) \mathcal{N}_{oldsymbol{ heta}}(\cdot | oldsymbol{x}_0, oldsymbol{x}_1), \ & (oldsymbol{x}_1, oldsymbol{x}_2, oldsymbol{x}_3) \sim \mathcal{N}_{oldsymbol{ heta}}(\cdot | oldsymbol{x}_0) \mathcal{N}_{oldsymbol{ heta}}(\cdot | oldsymbol{x}_0, oldsymbol{x}_1) \mathcal{N}_{oldsymbol{ heta}}(\cdot | oldsymbol{x}_0, oldsymbol{x}_1, oldsymbol{x}_2), \ & \vdots \\ & (oldsymbol{x}_1, oldsymbol{x}_2, ..., oldsymbol{x}_p) \sim \prod_{i=1}^p \mathcal{N}(\cdot | oldsymbol{x}_0, ..., oldsymbol{x}_{i-1}). \end{aligned}$$

By this means, we show that the reparameterization trick $x_i = m_{\theta}(x_{0:i-1}) + \sigma_{\theta}(x_{0:i-1})(z + rv_{\theta}(x_{0:i-1}))$ in (8) correctly generate in-distribution samples $x \sim \pi(\varphi)$.

B.2 Issue with (9): a divergent gaussian mean

Deriving (9). Recall that (9) presents the vanilla gradient of $\bar{\mathcal{J}}_{\alpha}(\theta) = \mathbb{E}_{\pi(x;\varphi)}[f(x)]$ w.r.t. θ , which is expressed as:

$$\nabla \bar{\mathcal{J}}_{\alpha}(\boldsymbol{\theta}) = \sum_{i=1}^{p} \mathbb{E}_{\pi(\boldsymbol{x};\boldsymbol{\varphi})} \left[f(\boldsymbol{x}) \frac{\partial}{\partial \boldsymbol{\theta}} \left(\frac{\partial \ln \mathcal{N}(\boldsymbol{x}_{i};\boldsymbol{\varphi}_{i})}{\partial \boldsymbol{\varphi}_{i}} \right) \right],$$

where $\varphi_i = \varphi_{\theta}(\boldsymbol{x}_{0:i-1})$. We are going to derive the term $\frac{\partial \ln \mathcal{N}(\boldsymbol{x}_i; \varphi_i)}{\partial \varphi_i}$. Notice that the partial derivative of $\pi(\boldsymbol{x}; \varphi) = \prod_{i=1}^p \mathcal{N}(\boldsymbol{x}_i; \varphi_i)$ w.r.t. φ can be derived as:

$$\frac{\partial \ln \pi(\boldsymbol{x}; \boldsymbol{\varphi})}{\partial \boldsymbol{\varphi}} = \frac{1}{\pi(\boldsymbol{x}; \boldsymbol{\varphi})} \frac{\partial \pi(\boldsymbol{x}; \boldsymbol{\varphi})}{\partial \boldsymbol{\varphi}} = \sum_{i=1}^{p} \frac{\partial \ln \mathcal{N}(\boldsymbol{x}_{i}; \boldsymbol{\varphi}_{i})}{\partial \boldsymbol{\varphi}_{i}}, \Rightarrow \frac{\partial \pi(\boldsymbol{x}; \boldsymbol{\varphi})}{\partial \boldsymbol{\varphi}} = \pi(\boldsymbol{x}; \boldsymbol{\varphi}) \sum_{i=1}^{p} \frac{\partial \ln \mathcal{N}(\boldsymbol{x}_{i}; \boldsymbol{\varphi}_{i})}{\partial \boldsymbol{\varphi}_{i}}.$$
(12)

Using the above, we can derive the partial derivatives $\partial \bar{\mathcal{J}}/\partial \varphi$:

$$\frac{\partial \bar{\mathcal{J}}}{\partial \boldsymbol{\varphi}_{i}} = \int_{\boldsymbol{x}} f(\boldsymbol{x}) \frac{\partial \pi(\boldsymbol{x}; \boldsymbol{\varphi})}{\partial \boldsymbol{\varphi}} d\boldsymbol{x} = \int_{\boldsymbol{x}} f(\boldsymbol{x}) \pi(\boldsymbol{x}; \boldsymbol{\varphi}) \sum_{i=1}^{p} \frac{\partial \ln \mathcal{N}(\boldsymbol{x}_{i}; \boldsymbol{\varphi}_{i})}{\partial \boldsymbol{\varphi}_{i}} d\boldsymbol{x} = \sum_{i=1}^{p} \mathbb{E}_{\pi(\boldsymbol{x}; \boldsymbol{\varphi})} \left[f(\boldsymbol{x}) \frac{\partial \ln \mathcal{N}(\boldsymbol{x}_{i}; \boldsymbol{\varphi}_{i})}{\partial \boldsymbol{\varphi}_{i}} \right].$$
(13)

Eventually, the gradient w.r,t. θ can be derived by directly applying the chain rule, which recovers (9).

The issue. Regarding a random sample $\mathbf{x}_i \in \mathbb{R}^d$, we refer to $\partial \ln \mathcal{N}(\mathbf{x}_i; \varphi_i) / \partial \varphi_i$ in (13) as the vanilla gradient of the log-likelihood of $\mathcal{N}(\mathbf{x}_i; \varphi_i)$. The biggest issue is perhaps that it potentially hinders the convergence of \mathbf{m}_i , which explains why 1) vanilla gradient is not popular and 2) some so-called ES variants proposed recently [23, 22] either update the distribution mean only or update the covariance matrix using gradient-free strategies. For an arbitrary $\mathcal{N}(\mathbf{x}_i; \varphi_i)$ where $\varphi_i^T = (\mathbf{m}_i^T, \text{vec}(\mathbf{C}_i)^T)$, and vec \cdot is the vectorization operator that stacks all the columns of an input matrix [61]. With a slight abuse of symbols, we consider in this and the next subsections that the mean \mathbf{m}_i and covariance matrix \mathbf{C}_i are constant parameters. The vanilla gradient regarding a random sample \mathbf{x}_i can be derived as [39]:

$$\frac{\partial \ln \mathcal{N}(\boldsymbol{x}_i; \boldsymbol{\varphi}_i)}{\partial \boldsymbol{\varphi}_i} = \begin{pmatrix} \frac{\partial \ln \mathcal{N}(\boldsymbol{x}_i; \boldsymbol{\varphi}_i)}{\partial \boldsymbol{m}_i} \\ \frac{\partial \ln \mathcal{N}(\boldsymbol{x}_i; \boldsymbol{\varphi}_i)}{\partial \operatorname{vec}(\boldsymbol{C}_i)} \end{pmatrix} = \begin{pmatrix} \boldsymbol{C}_i^{-1}(\boldsymbol{x}_i - \boldsymbol{m}_i) \\ \frac{1}{2} \operatorname{vec} \left(\boldsymbol{C}_i^{-1}(\boldsymbol{x}_i - \boldsymbol{\varphi}_i)(\boldsymbol{x}_i - \boldsymbol{\varphi}_i)^T \boldsymbol{C}_i^{-1} - \boldsymbol{C}_i^{-1} \right) \end{pmatrix}.$$
(14)

By eigenvalue decomposition, $C_i = Q\Lambda\Lambda Q^T$, where Λ is a diagonal matrix whose main diagonal consists of the square roots of C_i 's eigenvalues, and Q is an orthonormal matrix satisfying $Q^T = Q^{-1}$. x_i can thus be reparameterized by $x_i = m_i + Q\Lambda z_i$ where $z_i \sim \mathcal{N}(0, I)$. Consequently, we can rewrite

$$\frac{\partial \ln \mathcal{N}(\boldsymbol{x}_{i}; \boldsymbol{\varphi}_{i})}{\partial \boldsymbol{m}_{i}} = \overbrace{\boldsymbol{Q}^{-T} \boldsymbol{\Lambda}^{-1} \boldsymbol{\Lambda}^{-1} \boldsymbol{Q}^{-1}}^{=\boldsymbol{C}_{i}^{-1}} \underbrace{\boldsymbol{m}_{i} + \boldsymbol{Q} \boldsymbol{\Lambda} \boldsymbol{z}_{i}}_{=\boldsymbol{Q} \boldsymbol{\Lambda} \boldsymbol{Z}_{i}} - \boldsymbol{m}_{i}) = \overbrace{\boldsymbol{Q}^{-T} \boldsymbol{\Lambda}^{-1} \boldsymbol{\Lambda}^{-1} \boldsymbol{Q}^{-1} \boldsymbol{Q} \boldsymbol{\Lambda}}^{=\boldsymbol{I}} \boldsymbol{z}_{i} = \boldsymbol{Q} \boldsymbol{\Lambda}^{-1} \boldsymbol{z}_{i},$$
(15)

whose variance is:

$$\operatorname{Var}\left(\frac{\partial \ln \mathcal{N}(\boldsymbol{x}_i; \boldsymbol{\varphi}_i)}{\partial \boldsymbol{m}_i}\right) = \mathbb{E}\left[\left(\boldsymbol{z}_i - \widetilde{\mathbb{E}[\boldsymbol{z}_i]}\right)^T \boldsymbol{\Lambda}^{-1} \boldsymbol{\widetilde{\boldsymbol{Q}}}^T \boldsymbol{Q} \boldsymbol{\Lambda}^{-1} \left(\boldsymbol{z}_i - \mathbb{E}[\boldsymbol{z}_i]\right)\right] = \sum_{j=1}^d \frac{1}{\nu_j} \widetilde{\mathbb{E}[\boldsymbol{z}_j^2]} = \operatorname{Tr}(\boldsymbol{C}_i^{-1}),$$
(16)

where $z_i = (z_1, ..., z_d)^T$, ν_i is the *i*-th largest eigenvalue of C_i , $\mathbb{E}[z^j] = 1$ for all $j \in [d]$ is due to the mean of the chi-squared distribution, and $\text{Tr}(\cdot)$ denotes the trace of a matrix. Intuitively, during the search process, the entropy of the search distribution, i.e., the (log-)determinant of C_i , usually decreases, which is likely to increase $\text{Tr}(C_i^{-1})$, and therefore prevents m_i from staying in a stationary point. The phenomenon has been observed in [20] and rigorously discussed in [26].

B.3 Proof of Lemma 1 & interpretation of (10)

Define $\pi(\boldsymbol{x}; \boldsymbol{\varphi}) = \prod_{i=1}^p \mathcal{N}(\boldsymbol{x}_i; \boldsymbol{\varphi}_i)$ and $\boldsymbol{\varphi}_i = (\boldsymbol{m}_i^T, \text{vec } \boldsymbol{C}_i^T)^T$. Note that we treat \boldsymbol{m}_i and \boldsymbol{C}_i as constant parameters instead of mappings from $\boldsymbol{x}_{0:i-1}$. We introduce the definition of natural gradient and its geometric interpretation:

Definition 4 (Natural gradient [62]). Consider a distribution $\pi(\cdot; \varphi)$ that is differentiable w.r.t. its parameters φ , with the p.d.f. $\pi(x; \varphi)$. The natural gradient of any differentiable function $h(\varphi)$ w.r.t. φ is given by

$$\tilde{\nabla}h(\varphi) = \mathcal{F}(\varphi)^{-1}\nabla h(\varphi),\tag{17}$$

where and $\mathcal{F}(\varphi) = \mathbb{E}_{\pi(x;\varphi)}[\nabla \ln \pi(x;\varphi)\nabla \ln \pi(x;\varphi)^T]$ is referred to as the Fisher information matrix *w.r.t.* φ .

Proposition 2 (Geometric interpretation of natural gradient [25]). The natural gradient $\tilde{\nabla}h(\varphi)$ points in the direction δ that yields the greatest improvement of h, for a given distance between $\pi(\cdot; \varphi)$ and $\pi(\varphi + \delta)$ in Kullback-Leibler divergence. More precisely, let $\varphi \in \Phi$ be a point where $\|\tilde{\nabla}h(\varphi)\| > 0$, then

$$\boldsymbol{\delta}^* = \frac{\tilde{\nabla}h(\boldsymbol{\varphi})}{\|\tilde{\nabla}h(\boldsymbol{\varphi})\|} = \lim_{\epsilon \to 0^+} \frac{1}{\epsilon} \underset{\boldsymbol{\delta}}{\operatorname{argmax}} \ h(\boldsymbol{\varphi} + \boldsymbol{\delta}), s. \ t. \ \mathcal{KL}\left(\mathcal{N}(\pi(\boldsymbol{\varphi})) \parallel \mathcal{N}(\pi(\boldsymbol{\varphi} + \boldsymbol{\delta}))\right) \le \frac{\epsilon^2}{2}.$$
(18)

Of the above, **definition** 4 provides the form of a natural gradient, and **proposition** 2 suggests that a natural gradient identities the steepest ascent direction on Riemannian manifolds, and in the meanwhile, guarantees steady changes of π .

We prove Lemma 1 as follows:

Proof. First, the gradient of $\ln \pi(x; \varphi)$ is:

$$abla \ln \pi(oldsymbol{x};oldsymbol{arphi}) = rac{\partial \ln \pi(oldsymbol{x};oldsymbol{arphi})}{\partial oldsymbol{arphi}} = \left(rac{\partial \ln \mathcal{N}(oldsymbol{x}_1;oldsymbol{arphi}_1)}{\partial oldsymbol{arphi}_1}^T,...,rac{\partial \ln \mathcal{N}(oldsymbol{x}_p;oldsymbol{arphi}_p)}{\partial oldsymbol{arphi}_p}^T
ight)^T.$$

According to the definition of the Fis

$$\mathcal{F}(\varphi) = \mathbb{E}_{\pi(\boldsymbol{x};\varphi)} \begin{bmatrix} \frac{\partial \ln \mathcal{N}(\boldsymbol{x}_{1};\varphi_{1})}{\partial \varphi_{1}} \frac{\partial \ln \mathcal{N}(\boldsymbol{x}_{1};\varphi_{1})}{\partial \varphi_{1}}^{T}, & \cdots, & \frac{\partial \ln \mathcal{N}(\boldsymbol{x}_{1};\varphi_{1})}{\partial \varphi_{1}} \frac{\partial \ln \mathcal{N}(\boldsymbol{x}_{p};\varphi_{p})}{\partial \varphi_{p}}^{T} \\ \vdots, & \ddots, & \vdots \\ \frac{\partial \ln \mathcal{N}(\boldsymbol{x}_{p};\varphi_{p})}{\partial \varphi_{p}} \frac{\partial \ln \mathcal{N}(\boldsymbol{x}_{1};\varphi_{1})}{\partial \varphi_{1}}^{T}, & \cdots, & \frac{\partial \ln \mathcal{N}(\boldsymbol{x}_{p};\varphi_{p})}{\partial \varphi_{p}} \frac{\partial \ln \mathcal{N}(\boldsymbol{x}_{p};\varphi_{p})}{\partial \varphi_{p}}^{T} \end{bmatrix}.$$
(19)

Denoted by $\mathcal{F}_{ij} = \mathbb{E}_{\pi(\boldsymbol{x};\boldsymbol{\varphi})} \left[\frac{\partial \ln \mathcal{N}(\boldsymbol{x}_i;\boldsymbol{\varphi}_i)}{\partial \boldsymbol{\varphi}_i} \frac{\partial \ln \mathcal{N}(\boldsymbol{x}_j;\boldsymbol{\varphi}_j)}{\partial \boldsymbol{\varphi}_j}^T \right]$ the block entry of $\mathcal{F}(\boldsymbol{\varphi})$ on the *i*-th row and *j*-th column in (19), where $i \neq j$, then

$$\mathcal{F}_{ij} = \int_{x} \pi(x; \varphi) \frac{\partial \ln \mathcal{N}(x_{i}; \varphi_{i})}{\partial \varphi_{i}} \frac{\partial \ln \mathcal{N}(x_{j}; \varphi_{j})}{\partial \varphi_{j}}^{T} dx$$

$$= \int_{x} \prod_{k=1}^{p} \mathcal{N}(x_{k}; \varphi_{k}) \frac{\partial \ln \mathcal{N}(x_{i}; \varphi_{i})}{\partial \varphi_{i}} \frac{\partial \ln \mathcal{N}(x_{j}; \varphi_{j})}{\partial \varphi_{j}}^{T} dx$$

$$= \int_{x} \prod_{k=1, k \neq i \neq j}^{p} \mathcal{N}(x_{k}; \varphi_{k}) \frac{\partial \mathcal{N}(x_{i}; \varphi_{i})}{\partial \varphi_{i}} \frac{\partial \mathcal{N}(x_{i}; \varphi_{i})}{\partial \varphi_{i}} \frac{\partial \mathcal{N}(x_{j}; \varphi_{j})}{\partial \varphi_{j}}^{T} dx$$

$$= \int_{x_{1}} \dots \int_{x_{p}} \prod_{k=1, k \neq i \neq j}^{p} \mathcal{N}(x_{k}; \varphi_{k}) \frac{\partial \mathcal{N}(x_{i}; \varphi_{i})}{\partial \varphi_{i}} \frac{\partial \mathcal{N}(x_{j}; \varphi_{j})}{\partial \varphi_{j}}^{T} \frac{\partial \mathcal{N}(x_{j}; \varphi_{j})}{\partial \varphi_{j}}^{T} dx$$

$$= \prod_{k=1, k \neq i \neq j}^{p} \underbrace{\int_{x_{k}} \mathcal{N}(x_{k}; \varphi_{k}) dx_{k}}_{=1} \frac{\partial \mathcal{N}(x_{i}; \varphi_{i})}{\partial \varphi_{i}} \frac{\partial \mathcal{N}(x_{i}; \varphi_{i}) dx_{i}}{\partial \varphi_{j}} \frac{\partial \mathcal{N}(x_{j}; \varphi_{j})}{\partial \varphi_{j}}^{T} \frac{\partial \mathcal{N}(x_{j}; \varphi_{j}) dx_{j}}{\partial \varphi_{j}}^{T}$$

$$= 0.$$

$$= 0.$$

which means all the off-diagonal block entries are zero, and $\mathcal{F}(arphi)$ turns out to be a block-diagonal matrix.

which means all the off-diagonal block entries are zero, and
$$\mathcal{F}(\varphi)$$
 turns out to be a block-diagonal matrix. Furthermore, notice that $\mathcal{F}(\varphi_i) = \mathbb{E}_{\pi(\boldsymbol{x};\varphi)} \left[\frac{\partial \ln \mathcal{N}(\boldsymbol{x}_i;\varphi_i)}{\partial \varphi_i} \frac{\partial \ln \mathcal{N}(\boldsymbol{x}_i;\varphi_i)}{\partial \varphi_i}^T \right]$ for all $i \in [p]$, which implies:
$$\tilde{\nabla} \ln \pi(\boldsymbol{x};\varphi) = \mathcal{F}(\varphi)^{-1} \nabla \ln \pi(\boldsymbol{x};\varphi) = \begin{pmatrix} \mathcal{F}(\varphi_1)^{-1}, & \mathbf{0}, & \mathbf{0} \\ \mathbf{0}, & \ddots, & \mathbf{0} \\ \mathbf{0}, & \mathbf{0}, & \mathcal{F}(\varphi_p)^{-1} \end{pmatrix} \nabla \ln \pi(\boldsymbol{x};\varphi)$$

$$= \sum_{i=1}^p \mathcal{F}(\varphi_i)^{-1} \frac{\partial \ln \mathcal{N}(\boldsymbol{x}_i;\varphi_i)}{\partial \varphi_i}.$$
(21)

As \boldsymbol{x} follows $\pi(\cdot; \boldsymbol{\varphi})$, it is trivially unbiased. Therefore, we have shown that $\tilde{\nabla} \ln \pi(\boldsymbol{x}; \boldsymbol{\varphi})$ $\sum_{i=1}^{p} \boldsymbol{\mathcal{F}}(\boldsymbol{\varphi}_{i})^{-1} \frac{\partial \ln \mathcal{N}(\boldsymbol{x}_{i}; \boldsymbol{\varphi}_{i})}{\partial \boldsymbol{\varphi}_{i}}$.

Interpretion of (10). We can plug (21) into (10) and apply Monte-Carlo approximation to $\nabla \bar{\mathcal{J}}_{\alpha}(\theta)$, which yields:

$$\tilde{\nabla} \bar{\mathcal{J}}_{\alpha}(\boldsymbol{\theta}) = \mathbb{E}_{\pi(\boldsymbol{x};\boldsymbol{\varphi})} \left[f(\boldsymbol{x}) \frac{\partial}{\partial \boldsymbol{\theta}} \left(\tilde{\nabla} \ln \pi(\boldsymbol{x};\boldsymbol{\varphi}) \right) \right] = \frac{1}{\lambda} \sum_{i=1}^{\lambda} f(\boldsymbol{x}^{i}) \frac{\partial}{\partial \boldsymbol{\theta}} \left(\tilde{\nabla} \ln \pi(\boldsymbol{x}^{i};\boldsymbol{\varphi}^{j}) \right), \tag{22}$$

where $\varphi^j = (\varphi_{1j}^T, ..., \varphi_{pj}^T)^T$ and $\varphi_{ij} = \varphi_{\theta}(\boldsymbol{x}_{0:i-1}^j)$. Intuitively, the right-hand side of the above works as follows: first, sample a bunch of distributions $\pi(\varphi^1), ..., \pi(\varphi^p)$; then, for each of these distributions, sample a

random solution $x^j \sim \pi(\varphi^j)$; in the meanwhile, θ satisfies that $\varphi_{ij} = \varphi_{\theta}(x^j_{0:i-1})$; eventually, estimate the natural gradient of $\ln \pi(x^j; \varphi^j)$ w.r.t. φ^j using x^j . In brief, (10) amounts to aggregating the natural gradient of a set of sampled distributions $\pi(\varphi^1), ..., \pi(\varphi^p)$, and then back-propagating the gradient to θ through the chain rule.

B.4 Deriving the update rule (11)

(22) cannot be directly used in implementing the algorithm, as it 1) involves computing $\mathcal{F}(\varphi_i)^{-1}$, which is inefficient, and 2) does not specify how the gradient is back-propagated to θ through the chain rule. To this end, we first introduce Equation (24) of Akimoto *et al.* [39], which avoids the computation of $\mathcal{F}(\varphi_i)^{-1}$:

Proposition 3 (Natural gradient of a Gaussian). Consider a Gaussian random sample $\mathbf{x} \sim \mathcal{N}(\boldsymbol{\varphi})$ where $\boldsymbol{\varphi}_i = (\boldsymbol{m}_i^T, \text{vec}(\boldsymbol{C}_i)^T)^T$, the natural gradient of the log-likelihood $\ln \mathcal{N}(\boldsymbol{x}_i; \boldsymbol{\varphi}_i)$ is

$$\mathcal{F}(\boldsymbol{\varphi}_i)^{-1} \frac{\partial \ln \mathcal{N}(\boldsymbol{x}_i; \boldsymbol{\varphi}_i)}{\partial \boldsymbol{\varphi}_i} = \begin{pmatrix} \boldsymbol{x}_i - \boldsymbol{m}_i \\ vec\left((\boldsymbol{x}_i - \boldsymbol{m}_i)(\boldsymbol{x} - \boldsymbol{m}_i)^T - \boldsymbol{C}_i\right) \end{pmatrix}. \tag{23}$$

Define $m_i = m_{\theta}(\boldsymbol{x}_{0:i-1})$, $C_i = \sigma_i^2(\boldsymbol{I} + \boldsymbol{v}_i \boldsymbol{v}_i^T)$, $\sigma_i = \sigma_{\theta}(\boldsymbol{x}_{0:i-1})$, $\boldsymbol{v}_i = \boldsymbol{v}_{\theta}(\boldsymbol{x}_{0:i-1})$, and $\boldsymbol{y}_i = \boldsymbol{x}_i - \boldsymbol{m}_i$. According to the chain rule:

$$\frac{\partial}{\partial \boldsymbol{\theta}} \left(\mathcal{F}(\boldsymbol{\varphi}_i)^{-1} \frac{\partial \ln \mathcal{N}(\boldsymbol{x}_i; \boldsymbol{\varphi}_i)}{\partial \boldsymbol{\varphi}_i} \right) = \underbrace{J(\boldsymbol{m}_i)^T}_{=(\partial \boldsymbol{m}_i)^T} (\boldsymbol{x}_i - \boldsymbol{m}_i) + \frac{\partial \operatorname{vec} \boldsymbol{C}_i}{\partial \boldsymbol{\theta}}^T \operatorname{vec} \left((\boldsymbol{x}_i - \boldsymbol{m}_i)(\boldsymbol{x} - \boldsymbol{m}_i)^T - \boldsymbol{C}_i \right) \\
= J(\boldsymbol{m}_i)^T \boldsymbol{y}_i + \underbrace{\left(\frac{\partial \sigma_i}{\partial \boldsymbol{\theta}} \frac{\partial \operatorname{vec} \boldsymbol{C}_i}{\partial \sigma_i} + J(\boldsymbol{v}_i)^T \frac{\partial \operatorname{vec} \boldsymbol{C}_i}{\partial \boldsymbol{v}_i} \right)}_{=(\partial \operatorname{vec} \boldsymbol{C}_i / \partial \boldsymbol{\theta})^T} \operatorname{vec} \left(\boldsymbol{y}_i \boldsymbol{y}_i^T - \boldsymbol{C}_i \right),$$

where $J: \mathbb{R}^d \to \mathbb{R}^{d \times |\theta|}$ is the Jacobian matrix. In the following, we will expand the above terms one by one:

$$\frac{1}{2\sigma_{i}} \frac{\partial \operatorname{vec} \boldsymbol{C}_{i}}{\partial \sigma_{i}} \operatorname{vec} \left(\boldsymbol{y}_{i} \boldsymbol{y}_{i}^{T} - \boldsymbol{C}_{i} \right) = \operatorname{vec} (\boldsymbol{I} + \boldsymbol{v}_{i} \boldsymbol{v}_{i})^{T} \cdot \operatorname{vec} (\boldsymbol{y}_{i} \boldsymbol{y}_{i}^{T} - \boldsymbol{C}_{i})$$

$$= \operatorname{Tr} \left((\boldsymbol{I} + \boldsymbol{v}_{i} \boldsymbol{v}_{i}^{T}) \boldsymbol{y}_{i} \boldsymbol{y}_{i}^{T} \right) - \operatorname{Tr} \left((\boldsymbol{I} + \boldsymbol{v}_{i} \boldsymbol{v}_{i}^{T}) \boldsymbol{\sigma}_{i}^{2} (\boldsymbol{I} + \boldsymbol{v}_{i} \boldsymbol{v}_{i}^{T}) \right) \qquad (25)$$

$$= \operatorname{Tr} \left(\boldsymbol{y}_{i} \boldsymbol{y}_{i}^{T} \right) + \operatorname{Tr} \left(\boldsymbol{v}_{i} \boldsymbol{v}_{i}^{T} \boldsymbol{y}_{i} \boldsymbol{y}_{i}^{T} \right) - \sigma_{i}^{2} \operatorname{Tr} \left((\boldsymbol{I} + \boldsymbol{v}_{i} \boldsymbol{v}_{i}^{T})^{2} \right)$$

$$= \|\boldsymbol{y}_{i}\|^{2} + (\boldsymbol{v}_{i}^{T} \boldsymbol{y}_{i})^{2} - \sigma_{i}^{2} (d + 2\|\boldsymbol{v}_{i}\|^{2} + \|\boldsymbol{v}_{i}\|^{4});$$

and

$$\frac{\partial \operatorname{vec} \boldsymbol{C}_{i}}{\partial \boldsymbol{v}_{i}} \operatorname{vec} \left(\boldsymbol{y}_{i} \boldsymbol{y}_{i}^{T} - \boldsymbol{C}_{i} \right) \\
= \sigma_{i}^{2} \left(\boldsymbol{I} \otimes \boldsymbol{v}_{i} + \boldsymbol{v}_{i} \otimes \boldsymbol{I} \right)^{T} \left(\begin{array}{c} \underbrace{\boldsymbol{v}_{i} \boldsymbol{y}_{i}^{T}} \\ \boldsymbol{y}_{i} \otimes \boldsymbol{y}_{i} \end{array} - \operatorname{vec} \boldsymbol{C}_{i} \right) \\
= \sigma_{i}^{2} \left(\boldsymbol{I} \otimes \boldsymbol{v}_{i} + \boldsymbol{v}_{i} \otimes \boldsymbol{I} \right) \left(\boldsymbol{y}_{i} \otimes \boldsymbol{y}_{i} \right) - \sigma_{i}^{2} \left(\boldsymbol{I} \otimes \boldsymbol{v}_{i} + \boldsymbol{v}_{i} \otimes \boldsymbol{I} \right) \underbrace{\sigma_{i}^{2} \operatorname{vec}(\boldsymbol{I} + \boldsymbol{v}_{i} \boldsymbol{v}_{i}^{T}) = \operatorname{vec}(\boldsymbol{C}_{i})}_{\sigma_{i}^{2} \left(\operatorname{vec}(\boldsymbol{I}) + \boldsymbol{v}_{i} \otimes \boldsymbol{v}_{i} \right) \\
= \sigma_{i}^{2} \left(\left(\boldsymbol{v}_{i}^{T} \boldsymbol{y}_{i} \right) \boldsymbol{y}_{i} + \left\| \boldsymbol{y}_{i} \right\|^{2} \boldsymbol{v}_{i} \right) - 2\sigma_{i}^{4} \left(1 + \left\| \boldsymbol{v}_{i} \right\|^{2} \right) \boldsymbol{v}, \tag{26}$$

where \otimes denotes the Kronecker product [61]. Plugging (25) and (26) into (24) yields:

$$(24) = \mathbf{J}(\mathbf{m}_{i})^{T} \mathbf{y}_{i}$$

$$+ 2\sigma_{i} \left(\|\mathbf{y}_{i}\|^{2} + (\mathbf{v}_{i}^{T} \mathbf{y}_{i})^{2} - \sigma_{i}^{2} (d + 2\|\mathbf{v}_{i}\|^{2} + \|\mathbf{v}_{i}\|^{4}) \right) \frac{\partial \sigma_{i}}{\partial \boldsymbol{\theta}}$$

$$+ \sigma_{i}^{2} \mathbf{J}(\mathbf{v}_{i})^{T} \left(\mathbf{v}_{i}^{T} \mathbf{y}_{i} \mathbf{y}_{i} + \|\mathbf{y}_{i}\|^{2} \mathbf{v}_{i} - 2\sigma_{i}^{2} \left(1 + \|\mathbf{v}_{i}\|^{2} \right) \mathbf{v} \right).$$

$$(27)$$

Consider a sample x^j , define $m_{ij} = m_{\theta}(x^j_{0:i-1})$, $\sigma_{ij} = \sigma_{\theta}(x^j_{0:i-1})$, $v_{ij} = v_{\theta}(x^j_{0:i-1})$, and $y_{ij} = x^j_i - m_{ij}$. Eventually, for each $j \in [\lambda]$ substituting (27) into (22) yields (11).

B.5 More on the weight values

The rank-dependent weights are also known as the use of utility [26, 25] or fitness shaping [20]. The rationale behind the weights in this paper, i.e., $w_1 \ge ... \ge w_\lambda$ and $w_j = \ln(\lfloor \frac{\lambda}{2} + \frac{1}{2} \rfloor) - \ln j$, is that they decrease

sub-linearly with the ranks: solutions before the median will be assigned positive weights, while those after (including the median itself) will be assigned negative weights, and no one will be assigned a zero weight. Separating the weights into positive and negative values is equivalent to using a reward baseline in many practical reinforcement learning methods. Note that in most CMA-ES variants [27, 29, 56], the second half of $\{x^j\}_{j=1}^p$ is discarded by default, especially when updating the Gaussian mean. This is because using inferior solutions implicitly imposes too strong a regularity assumption on a black-box objective, which may not be true. A counterexample is xNES, which uses the inferior solutions but normalizes their weights to $-1/\lambda$. However, we adopt all solutions to estimate due to the well-known data-hungry nature of neural networks.

B.6 Design of the set model

We use a feed-forward neural network as the set model. There are four hidden layers, each with a size of 1024. In order to input $x_{0:i-1}$ into the model, we construct

$$(\widehat{\boldsymbol{x}_{1}^{T}, \boldsymbol{x}_{2}^{T}, ..., \boldsymbol{x}_{i-1}^{T}}, \widehat{\text{nil}, ..., \text{nil}}, \widehat{\boldsymbol{1}, ..., 1}, \widehat{\boldsymbol{0}, ..., 0}, \widehat{\boldsymbol{x}_{0}})^{T},$$

$$(28)$$

where nil is a placeholder, 1 on the (n+j)-th $(1 \le j \le n)$ dimension indicates that the j-th input is not nil, and vice versa. Consequently, the size of the input layer is 2n+M. The output layer, which outputs $(\boldsymbol{m}_i^T, \sigma_i, \boldsymbol{v}_i^T)^T$, is of size 2d+1. We use the leaky ReLU function as the activation in the hidden layers, which is defined as $f^{\text{lr}}(\omega) = \max(\omega, 0) + 0.01 \min(0, \omega)$. In order to generate $\boldsymbol{m}_i, \boldsymbol{v}_i \in \mathbb{R}^d$, no activation is used in the output layer. To guarantee $\sigma_i > 0$, we take the absolute value of the (d+1)-th output dimension. The set model is trained using Adam, with a learning rate of $\eta = 10^{-3}$. Compared to SGD (stochastic gradient ascent), the adaptive momentum of Adam accumulates historical gradient information, enabling more accurate gradient estimation and significantly reducing the number of samples required.

B.7 Overall computational complexity

Consider a set model, i.e., a feed-forward neural network, with t hidden layers, and the sizes of the input, output, and hidden layers are 2n+M, 2d+1, and s, respectively. One can derive the space complexity of the network, as well as the time complexities of the feed-forward and back-propagation processes, which are all $\Theta(ts^2+(n+M+d)s)$. Since we are only interested in n and d, we can further simplify the complexity as $\Theta(n+d)$. We can easily imply that the space complexity of Neural-ES is $\Theta(n+d)$ as well, as the entire search distribution is compressed into the model.

The time complexity of Neural-ES stems from two sources: 1) sampling and 2) updating $\boldsymbol{\theta}$. To sample a component \boldsymbol{x}_i , it takes $\Theta(n+d)$ time to generate a $\boldsymbol{\varphi}_i = \boldsymbol{\varphi}_{\boldsymbol{\theta}}(\boldsymbol{x}_{0:i-1})$, which corresponds to the feed-forward process, and $\Theta(d)$ time to generate an \boldsymbol{x}_i according to (8). To generate a complete $\boldsymbol{x} = (\boldsymbol{x}_1^T, ..., \boldsymbol{x}_p^T)^T$, (8) needs to be performed p times. Therefore, the overall time complexity for sampling a $\boldsymbol{x} \sim \pi$ is $p\Theta(n+d) + p\Theta(d) = \Theta(pn)$, as n = pd.

To update $\boldsymbol{\theta}$, we need to compute (27). Within the equation, the computation of $\boldsymbol{J}(\boldsymbol{m}_i)$, $\frac{\partial \sigma_i}{\partial \boldsymbol{\theta}}$ and $\boldsymbol{J}(\boldsymbol{v}_i)$ takes a total of $\Theta(n+d)$ time, which corresponds to the back-propagation process; every matrix-vector multiplication takes $\Theta(n+d)*\Theta(d)=\Theta(nd+d^2)$ time; in addition, the computation of $\|\boldsymbol{y}_i\|^2$, $\boldsymbol{v}_i^T\boldsymbol{y}_i$ and $\|\boldsymbol{v}_i\|^2$ takes $\Theta(d)$ time. To sum up, the time complexity of (27) is $\Theta(n+d)+\Theta(nd+d^2)+\Theta(d)=\Theta(nd+d^2)$. In addition, (27) needs to be performed p times regarding a complete $\boldsymbol{x}=(\boldsymbol{x}_1^T,...,\boldsymbol{x}_p^T)^T$, which takes $p\Theta(nd+d^2)=\Theta(n^2+nd)=\Theta(n^2)$ time. Note that $\Theta(n^2)$ also represents the time complexity in the update of EPSL [15]. $\Theta(n^2)$ is indeed a near-optimum one can expect when updating $\boldsymbol{\theta}$, because $\frac{\partial \boldsymbol{\varphi}}{\partial \boldsymbol{\theta}}^T \frac{\partial \mathcal{J}}{\partial \boldsymbol{\varphi}}$ achieves $\Theta(n^2)$ time only when both $\boldsymbol{\varphi}$ and $\boldsymbol{\theta}$ scale linearly with n.

A typical counterexample is the application of other existing ES variants, such as xNES, to solve the black-box PSL problem. In this case, the space complexity will increase to $\Theta(n^2)$, the time complexity of sampling will increase to $\Theta(n^2)$, the time complexity of computing the partial derivative $\partial \bar{\mathcal{J}}_{\alpha}(\boldsymbol{\theta})/\partial \varphi$ will increase to $\Theta(n^2)$, and eventually computing the gradient $\nabla \bar{\mathcal{J}}_{\alpha}(\boldsymbol{\theta})$ as well as updating $\boldsymbol{\theta}$ will cost $\Theta(n^3)$ time or higher. In contrast, Neural-ES achieves $\Theta(n)$ space complexity, $\Theta(pn)$ time complexity of sampling a solution, and $\Theta(n^2)$ time complexity of updating $\boldsymbol{\theta}$. Therefore, we can conclude that Neural-ES is a time-efficient approach.

C More details on the experiments

C.1 Proposed BBO-PSL benchmark suite

A test problem for assessing the PSL algorithms should satisfy the following two requirements:

- Non-separability, which means $\operatorname{argmin}_{\boldsymbol{x}} f_i(\boldsymbol{x}) \neq (\operatorname{argmin}_{x_1} f_i(x_1, ...), ..., \operatorname{argmin}_{x_n} f_i(..., x_n))^T$ for all $i \in [m]$. This is a *conditio sine qua non*, because separable problems, which are rarely the practical case, cannot assess the ability to handle complex dimension dependency.
- Analytical PFs and complex PSs: where the former means that the ground-truth PF and PS should be
 expressed in closed forms, and the latter suggests that the Pareto optimal solutions should not be, e.g.,
 linearly distributed.

Surprisingly, few of the existing benchmark suites have satisfied both requirements. For example, the popular DTLZ problems [63] satisfy neither of them: they are separable, with simple PSs located on the boundary of the search space. Despite their complex PS shapes, the UF [43] and LZ [64] instances are separable. Though providing non-separable instances, the bi-objective BBOB problems [44] lack analytical PFs & PSs. The LS-MOP [45] focusing on large-scale multiobjective problems does not feature complex PSs, and most of its instances are separable or partially separable. An exception would be the recently proposed ZCAT suite [46], which, however, features non-simplex-like PFs and falls beyond the scope of this paper.

For these reasons, we design a novel benchmark suite based on the following theorem, which is also the design principle of the popular UF and LZ problems:

Theorem 1 (Li & Zhang [64]). Consider a MOP in (1) where

$$f_i(\boldsymbol{x}) = f_i^{pf}(\boldsymbol{x}_I) + f^{dis}(\boldsymbol{x}_{II} - \boldsymbol{f}^{ps}(\boldsymbol{x}_I)), \tag{29}$$

 $i=1,...,M,~~\boldsymbol{x}_I=(\mathbf{x}_1,...,\mathbf{x}_{M-1}),~~\boldsymbol{x}_{II}=(\mathbf{x}_M,...,\mathbf{x}_n),~~\boldsymbol{x}\in\mathcal{X},~~\mathcal{X}=\prod_{j=1}^n[a_j,b_j]\subset\mathbb{R}^n,~~f_i^{pf}:\prod_{j=1}^{M-1}[a_j,b_j]\to\mathbb{R},~~\boldsymbol{f}_j^{ps}:\prod_{j=1}^M[a_j,b_j]\to\mathbb{R}_+^{n-M+1},~~and~~f^{dis}:\prod_{j=1}^{n-M+1}[a_j,b_j]\to\mathbb{R}_+.~~Assume~~I)$ f^{dis} reaches the minimal of 0 at $\boldsymbol{0}$, which means $f^{dis}(\boldsymbol{x})\geq f^{dis}(\boldsymbol{0})=0,~~\forall \boldsymbol{x}\in\mathbb{R}^n,~and~~2)$ the following MOP has a PF and PS, which are denoted by PF* and PS*,

$$\underset{\boldsymbol{x}_I \in \prod_{I=1}^{M-1} [a_i, b_i]}{\text{minimize}} (f_1^{pf}(\boldsymbol{x}_I), ..., f_M^{pf}(\boldsymbol{x}_I))^T.$$
(30)

Then, 1) the PF of $\mathbf{F}(\mathbf{x})$ is PF^* , and 2) the PS of $\mathbf{F}(\mathbf{x})$ is $\{(\mathbf{x}_I, \mathbf{x}_{II})^T | \mathbf{x}_{II} = \mathbf{f}^{ps}(\mathbf{x}_I), \mathbf{x}_I \in PS^*\}$.

Of the above, $f_i^{\rm pf}$, ${\bf f}^{\rm ps}$, and $f^{\rm dis}$ are referred to as the PF, PS, and distance functions, as they determine the shapes of the PF and PS manifolds as well as the difficulty of optimizing ${\bf F}({\bf x})$, respectively. With **Theorem 1**, analytical PFs and complex PSs can be implemented by designing proper $f_i^{\rm pf}$ and ${\bf f}^{\rm ps}$, and non-separability can be implemented by introducing non-separable functions that achieve the minimum of zero at ${\bf x}={\bf 0}$.

We design instances in the proposed benchmark suite as follows. All the instances employ the rotated ellipsoidal function as the distance function, which, considering an input x_{II} , is expressed as:

$$f^{\text{rel}}(\boldsymbol{x}_{II}; \boldsymbol{\mathcal{R}}) = \boldsymbol{x}_{II}^T \boldsymbol{\mathcal{R}} \boldsymbol{\Lambda} \boldsymbol{\mathcal{R}}^T \boldsymbol{x}_{II}, \tag{31}$$

where \mathcal{R} is a (n-M+1)-dimensional orthonormal matrix, and $\mathbf{\Lambda}$ is a (n-M+1)-dimensional diagonal matrix whose i-th diagonal entry is $c^{\frac{i-1}{n-M}}$. Particularly, c is called the condition number [53], which denotes the ratio between the largest and smallest eigenvalues of a Hessian, and typically controls the optimization difficulty; a larger c yields a more difficult optimization problem. \mathcal{R} can be constructed by applying the Gram-Schmidt process to a random square matrix with standard normally distributed entries. All the bi-objective instances take the following form:

$$\boldsymbol{F}(\boldsymbol{x}) = \begin{cases} f_1^{\text{pf}}(x_1) + f^{\text{rel}} \boldsymbol{x}_{II} - \boldsymbol{f}^{\text{ps}}(x_1) \boldsymbol{\mathcal{R}} \\ f_2^{\text{pf}}(x_1) + f^{\text{rel}} \boldsymbol{x}_{II} - \boldsymbol{f}^{\text{ps}}(x_1) \boldsymbol{\mathcal{R}}' \end{cases},$$
(32)

where the PF function is $f^{pf}(x_1) = (x_1, 1 - \sqrt{x_1})^T$. All the tri-objective instances take the following form:

$$\boldsymbol{F}(\boldsymbol{x}) = \begin{cases} f_{1}^{\text{pf}}(x_{1}, x_{2}) + f^{\text{rel}}\boldsymbol{x}_{II} - \boldsymbol{f}^{\text{ps}}(x_{1}, x_{2})\boldsymbol{\mathcal{R}} \\ f_{2}^{\text{pf}}(x_{1}, x_{2}) + f^{\text{rel}}\boldsymbol{x}_{II} - \boldsymbol{f}^{\text{ps}}(x_{1}, x_{2})\boldsymbol{\mathcal{R}}' \\ f_{3}^{\text{pf}}(x_{1}, x_{2}) + f^{\text{rel}}\boldsymbol{x}_{II} - \boldsymbol{f}^{\text{ps}}(x_{1}, x_{2})\boldsymbol{\mathcal{R}}'' \end{cases}, \text{ where } \begin{cases} f_{1}^{\text{pf}}(x_{1}, x_{2}) = \cos(0.5\pi x_{1})\cos(0.5\pi x_{2}) \\ f_{2}^{\text{pf}}(x_{1}, x_{2}) = \cos(0.5\pi x_{1})\sin(0.5\pi x_{2}) \\ f_{3}^{\text{pf}}(x_{1}, x_{2}) = \sin(0.5\pi x_{1}) \end{cases}$$

$$(33)$$

and \mathcal{R} , \mathcal{R}' and \mathcal{R}'' denote three different rotation matrices.

Eventually, eight instances, F1 to F8, are listed in Table 2. F1 to F4 are bi-objective problems, while F5 to F8 are tri-objective. The search space for the bi-objective instances is $[0,1] \times [-1,1]^{n-1}$, and is $[0,1]^2 \times [-2,2]^{n-2}$ for the tri-objective ones. The condition number c is 100 in F1 to F4, and is 2 in F5 to F8. Their PS manifolds in the $(x_1 - x_2 - x_3)$ subspace are displayed in Fig. 8. In short, the proposed suite features non-separable and anisotropic distance functions, covering diverse nonlinear PS manifolds.

Table 2: The proposed BBO-PSL benchmark suite.

ID	M	$f^{ m ps}$
F1		$f_i^{\text{ps}}(x_1) = 0.75(1 - \psi_i)x_1 * \begin{cases} \cos(2\pi x_1), & \text{if } i \text{ is even,} \\ \sin(2\pi x_1), & \text{otherwise} \end{cases}$
F2	2	$f_i^{\text{ps}}(x_1) = \begin{cases} (\psi_i - 1)(x_1^2 - 2x_1 + 0.5), & \text{if } i \text{ is even,} \\ x_1^{1+\psi_i} - 0.5, & \text{otherwise} \end{cases}$
F3		$f_i^{\text{ps}}(x_1) = (1 - \psi_i)(2x_1 - 1)^3 + \psi_i(2x_1 - 1)$
F4		$f_i^{\text{ps}}(x_1) = 2x_1^{0.5+1.5\psi_i} - 1$
F5		$f_i^{\text{ps}}(x_1, x_2) = \xi_i \left(x_1^2 (1 - x_2) + (1 - x_1^2) x_2 - \frac{1}{2} \right)$
F6	3	$f_i^{\text{ps}}(x_1, x_2) = 0.5\xi_i \cos(\pi \frac{x_1 + x_2}{2}) \cos(\pi x_1 - x_2)$
F7		$f_i^{\text{ps}}(x_1, x_2) = 0.5\xi_i \left(x_2(1 - x_1^2) + (1 - x_2) \frac{x_1^2}{2} - 0.5 \right)$
F8		$f_i^{\text{ps}}(x_1, x_2) = 2\xi_i(x_1 - x_2)(x_1 + x_2 - 1)$

 $f_i^{\mathrm{ps}}(\cdot)$ denotes the *i*-th output of f^{ps} , $\psi_i = \frac{i-1}{n-2}$, and $\xi_i = \frac{n-i+1}{n-2}$.

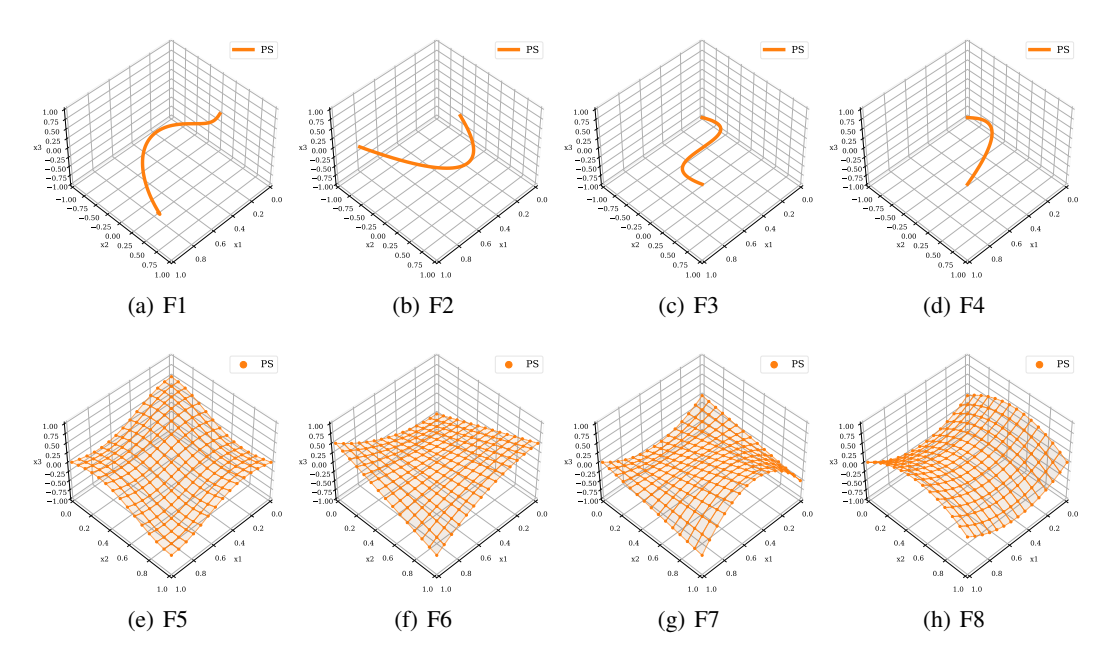


Figure 8: Ground-truth PS manifolds of the proposed problem instances.

C.2 More about the configurations

Compared algorithms. The two MOEAs used in the experiments, namely LMO-CSO and IM-MOEA/D, are implemented in the open-source PlatEMO library [65] 4 . Their hyperparameters are configured to their default values. The set models of EPSL and EPSL-R1 use the same hidden-layer structure as Neural-ES. Bernoulli smoothing, antithetic sampling, and smooth Tchebycheff of EPSL are deactivated for a fair comparison. The most dominating hyperparameters of Neural-ES are p, N, and λ . While $\lambda = 4 + \lfloor 3 \ln n \rfloor$ is a typical setup for most ES algorithms [19, 28], we reduce it to a half due to the large number of sampled subproblems $\{g(\cdot; \boldsymbol{\alpha}^k)\}_{k=1}^N$. We will discuss p and p in Section C.4. We use the popular Penalty-based Boundary Intersection (PBI) [8] as the aggregation function:

$$g_{\boldsymbol{u}}^{pbi}(\boldsymbol{F}; \boldsymbol{\alpha}) = D_1 + \rho D_2$$
, where
$$\begin{cases} D_1 = \frac{1}{\|\boldsymbol{\alpha}\|} \|(\boldsymbol{u} - \boldsymbol{F})^T \boldsymbol{\alpha}\| \\ D_2 = \|\boldsymbol{F} - \boldsymbol{u} + D_1 \boldsymbol{\alpha}\|, \end{cases}$$

F is a point in the objective space, $u \in \mathbb{R}^M$ is a reference point satisfying $u \le (\inf f_1(x), ..., \inf f_M(x))^T$, D_1 is the distance from u to the projection of u onto u and u is the distance from u to the projection of u onto u and u is the distance from u to the projection of u onto u and u is the distance from u to the projection of u onto u is the distance from u to the projection of u one approaches the underlying PF, while minimizing u is the distance from u to the projection of u one approaches the underlying PF, while minimizing u is the distance from u to the projection of u one approaches the underlying PF, while minimizing u is the distance from u to the projection of u one approaches the underlying PF, while minimizing u is the distance from u one approaches the underlying PF, while minimizing u is the distance from u one approaches the underlying PF, while minimizing u is the distance from u one approaches the underlying PF, while minimizing u is the distance from u one approaches the underlying PF, while minimizing u is the distance from u one approaches the underlying PF, while minimizing u is the distance from u one approaches the underlying PF.

⁴https://github.com/BIMK/PlatEMO

with the preference balpha. The parameter $\rho > 0$ trades off D_1 and D_2 . Although the Tchebycheff function [8] is also widely used, we have not considered it because we observe that its use can decrease solution diversity when solving tri-objective MOPs, which further leads to premature convergence of the set model.

Performance metrics. The Inverted Generational Distance (IGD) [48] is used for assessing the algorithms' performance, with a smaller value indicating better performance. Denoted by \widehat{PF} and PF a subset of the ground-truth PF, and PF an approximation by an algorithm, the IGD of PF is defined as the total distance from every point in PF to \widehat{PF} , and can be expressed as:

$$IGD(PF,\widehat{PF}) = \frac{1}{|\widehat{PF}|} \sum_{\mathbf{F}^* \in \widehat{PF}} \min_{\mathbf{F} \in PF} ||\mathbf{F} - \mathbf{F}^*||_2.$$

Intuitively, IGD measures the distance from each point F^* in the ideal set \widehat{PF} , to the closest F in the approximation set PF. When imposing ideal properties on \widehat{PF} , the IGD is minimized only when PF spreads widely and evenly. Otherwise, there will always be some $F^* \in \widehat{PF}$ that remains distant from PF, resulting in a large IGD.

Additionally, hypervolume (HV) is also used to evaluate algorithms in Section 5.3 where IGD values are unavailable. It measures the volume of a specific region in the objective space, which is between a solution set and a reference point, with a larger value indicating better performance. It is given by:

$$HV_{\boldsymbol{u}}(S) = \text{Vol}\{\boldsymbol{y}|\exists \boldsymbol{x} \in S, \boldsymbol{F}(\boldsymbol{x}) \prec \boldsymbol{y} \prec \boldsymbol{u}\}$$

where S is a solution set, u is a reference point in the F-space, Vol computes the volume of a set, and \prec denotes Pareto dominance. The volume always increases when the solution set approaches the ground truth PF more closely or spreads more widely across the PF, as both cases stretch the region.

Experiment configurations. We limit the size of \widehat{PF} to be 300 and 900 for the bi- and tri-objective instances, respectively. Each algorithm repeatedly solves each BBO-PSL instance 21 times, using a different random seed each time. For the three PSL algorithms, we evaluate their *testing performance*. Specifically, we input a large number of preferences into a trained set model, which yields the same number of distributions; from each distribution, we randomly sample a solution, the collection of which form the *testing solution set*; finally, we measure the IGD value of the set and refer it as the *testing IGD value*. The number of input preferences, i.e., the size of the testing solution set, is 900 and 4950 for the bi- and tri-objective instances, respectively. The MOEAs directly optimize the same number of solutions, and the IGD value of the final population is measured. Meanwhile, we track the convergence of the PSL algorithms during training, in terms of the IGD values of the *training solution set*. The training solution set at a certain iteration comprises the best solutions found so far for a set of evenly distributed subproblems. In light of the computational efficiency, its capacity is slightly smaller than the testing solution set, which is 100 and 300 for the bi- and tri-objective instances, respectively. To examine the scalability of the algorithms with increasing dimensions, we vary n from 32 to 1024. The evaluation budget is 4000n and 2000n for bi- and tri-objective instances. The bi-objective instances are given a larger budget because their condition numbers are higher, which implies greater difficulties.

C.3 More experiment results

Numerical results. The numerical results for Fig. 4 are listed in Table 3. The Mann-Whitney U test at a 95% confidence level is applied to statistically compare the algorithms. Neural-ES performs the best in all the instances, ranging from n=64 to 1024. The results conform to those in Fig. 4. Note that the results of LMO-CMO and IM-MOEA/D are obtained through directly optimizing the problems, while the results of the three PSL algorithms represent their test-time generalization outcomes. This indicates that even the testing performance of Neural-ES surpasses that of the MOEAs in terms of optimization results.

Approximate PF manifolds. Fig. 9 demonstrates the approximate PF manifolds by all five algorithms, on all the BBO-PSL instances. In all cases, the PFs approximated by Neural-ES dominate most areas of those approximated by the other algorithms, which conforms to Fig. 5. It appears that F3 and F4 are more challenging than F1 and F2, and F8 is more demanding than F5 to F7, indicating that the shape of the PS manifolds significantly influences the optimization difficulty. It can be observed that Neural-ES closely approximates the ground-truth PFs of all bi-objective instances, which highlights the learning capability of black-box PSL algorithms, particularly Neural-ES. However, the approximation results are inferior in the bi-objective instances, due to their significantly higher condition number. This confirms that the condition number of the distance function notably impacts optimization difficulty, which existing benchmark suites have neglected. Once again, the approximate PFs of Neural-ES and the other two PSL algorithms are produced during testing time, while those of LMO-CSO and IM-MOEA/D are direct optimization results. This suggests that the generalization ability of Neural-ES surpasses that of some state-of-the-art MOEAs.

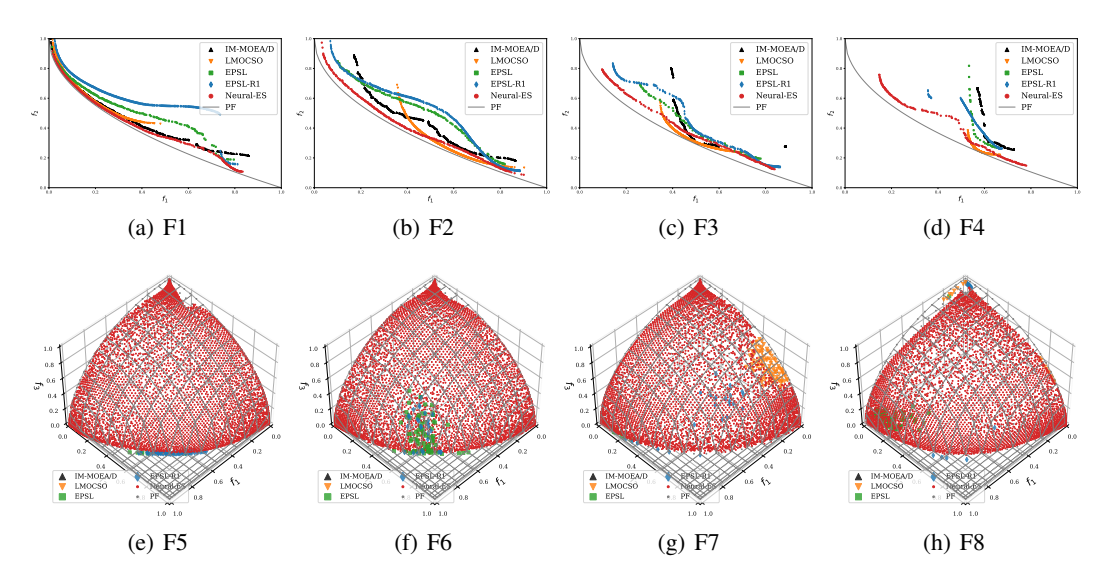


Figure 9: Testing-time PFs approximated by the algorithms, with n=256. For better visualization, only non-dominated solutions are presented for F5 to F8.

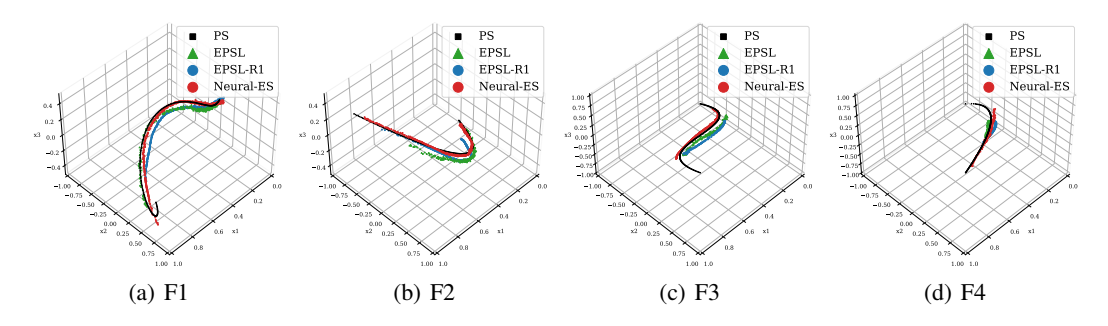


Figure 10: Testing-time PSs approximated by the PSL algorithms, on F1 to F4, with n=512.

Approximate PS manifolds. We focus on the PSL algorithms' ability to learn the PS manifolds. LMO-CSO and IM-MOEA/D are excluded as they do not possess such ability. The approximate PSs on the bi-objective F1 to F4 are plotted in Fig. 10. Neural-ES generates the most accurate PSs in all four cases, as the red curves align the closest to the ground-truth. It can be observed that F3 and F4 are more challenging than F1 and F2, as they have higher levels of non-linearity. The approximate PSs on the tri-objective F5 to F8 are plotted in Figs. 11 to 14. Neural-ES and EPSL-R1 generate closer and more uniform approximations than EPSL in all four cases. Although Neural-ES only slightly outperforms EPSL-R1 in the solution space, their performance gap is significant, because most solutions of Neural-ES dominate those of EPSL-R1 in the objective space, as shown in Fig. 9.

Convergence. Fig. 15 demonstrates the convergence trajectories of the three PSL algorithms. LMO-CSO and IM-MOEA/D are not involved due to their differing sample sizes during each iteration. The results conform to Fig. 3. Noticeably, EPSL-R1 converges slightly faster than EPSL in F1 to F4; however, instances F5 to F8 do not reflect its advantage. This is because F1 to F4 have a much higher condition number of 100, than F5 to F8, which have a condition number of 2. Evidently, dealing with the dimensional dependencies becomes more challenging as the condition number increases. Once again, existing benchmark suites overlook this issue, necessitating the proposal of the BBO-PSL suite. In all the instances, Neural-ES establishes a performance lead over EPSL and EPSL-R1 during the early stages, extending the performance gap throughout the search process, underscoring its superiority in handling dimensional dependencies.

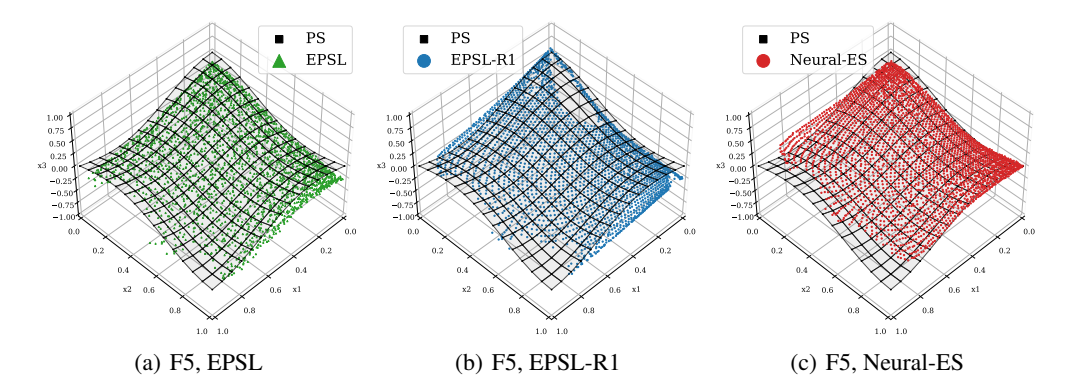


Figure 11: Testing-time PSs approximated by the PSL algorithms, on F5, with n = 128.

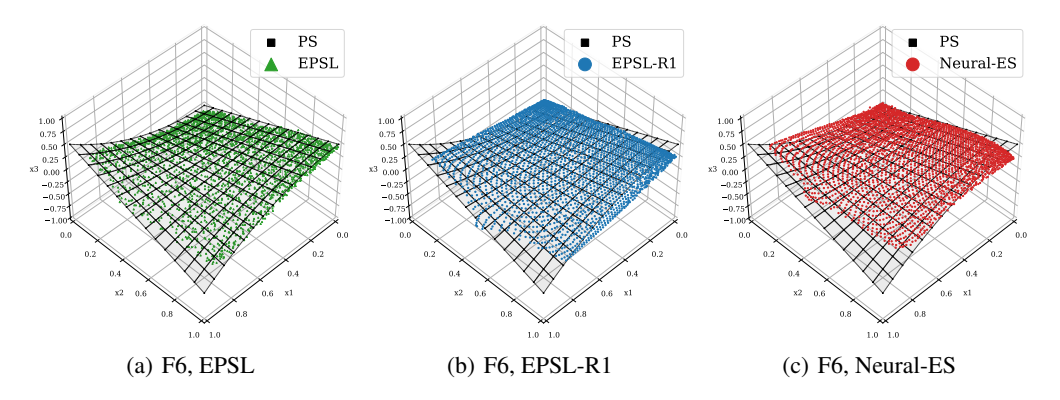


Figure 12: Testing-time PSs approximated by the PSL algorithms, on F6, with n = 128.

C.4 Sensitivity analyses

Intuitively, the number of partitions, p, and the number of sampled subproblems, N, are closely linked to the performance of Neural-ES. To determine their optimal setups as well as to observe how they vary with the increasing problem dimension n, we conducted the following two independent experiments:

- Investigating p: we apply $p \in \{64, 32, 16, 8, 4\}$ to solve F4 and F6, and meanwhile, fix $N = \lfloor 5n/16 \rfloor$.
- Investigating N: we apply $N \in \{10, 20, 40, 80, 160, 320\}$ to solve F4 and F6, and meanwhile, fix p = 16.

In the experiments, the dimensions of F4 and F6 range from 64 to 512. The two selected instances serve as the representative bi- and tri-objective BBO-PSL instances, which are expected to provide the most neutral observations. The experiment results, in terms of the final IGD values, are recorded in Fig. 16.

We can make the following observations:

- Regarding Figs. 16(a) and 16(b), the number of partitions p positively correlates to the problem dimension n. This is reasonable as a larger p yields more decomposed Gaussians, and therefore a stronger ability to handle dimensional dependencies. The results validate the efficacy of the novel dependency handling technique presented in this paper (i.e., Equation (6)).
- Regarding Figs. 16(c) and 16(d), the highlighted main diagonals of the figures indicate the trade-offs between N and Neural-ES: either too large or too small a sample size worsens the performance. This is reasonable because, on the one hand, a too large N consumes a significant portion of the evaluation budget; on the other hand, a too small N results in inaccurate gradient estimates.

To balance computational efficiency and performance, we adopt p=16. It can be observed from Figs. 16(c) and 16(d) that the optimal N is roughly $\lfloor 5n/16 \rceil$. To date, we have justified the hyperparameter settings presented in this paper.

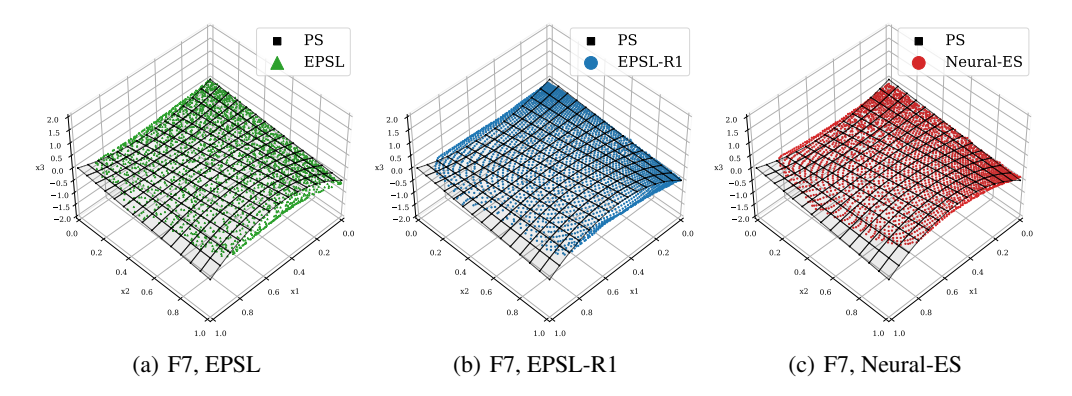


Figure 13: Testing-time PSs approximated by the PSL algorithms, on F7, with n = 128.

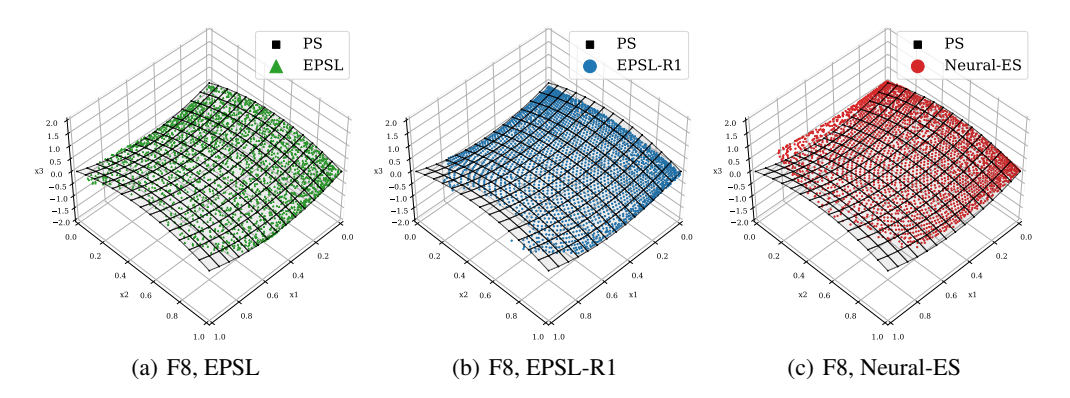


Figure 14: Testing-time PSs approximated by the PSL algorithms, on F8, with n = 128.

C.5 Runtime analyses

We have conducted an extensive evaluation of computational efficiency across all compared algorithms using two 1024-dimensional instances (F1 and F5) from our BBO-PSL suite. The evaluation budget remained the same as before, at 4,000n for F1 and 2,000n for F5. The results are reported in Table 4.

Comparing the PSL algorithms with the traditional MOEAs, we can observe that the former run faster, or at least as fast, as the latter. This is because most MOEAs require advanced techniques to maintain population diversity and address slow convergence, such as the RVEA-based environmental selection in LMO-CSO and the Gaussian process modeling in IM-

Table 4: Wall-clock time (in minutes).

	LMO-	IM-	EPSL	EPSL-	Neural-
	CSO	MOEA/D	Erst	R1	ES
F1	16.9	17.4	7.8	12.2	17.4
F5	23.9	15.2	5.1	7.4	9.5

MOEA/D. Most, if not all, of these techniques come with high overhead and scale poorly with increasing population sizes. In contrast, the PSL paradigm does not rely on any of these techniques. Despite introducing neural networks, the PSL algorithms turn out to run surprisingly faster, or at least equally fast, when compared to traditional MOEAs.

While Neural-ES shows a marginally higher runtime compared to the other two PSL algorithms, due to its more complex search distribution, it achieves much faster convergence in terms of the number of generations required. The faster convergence likely offsets its marginally higher computational cost per generation, making it advantageous for practical applications.

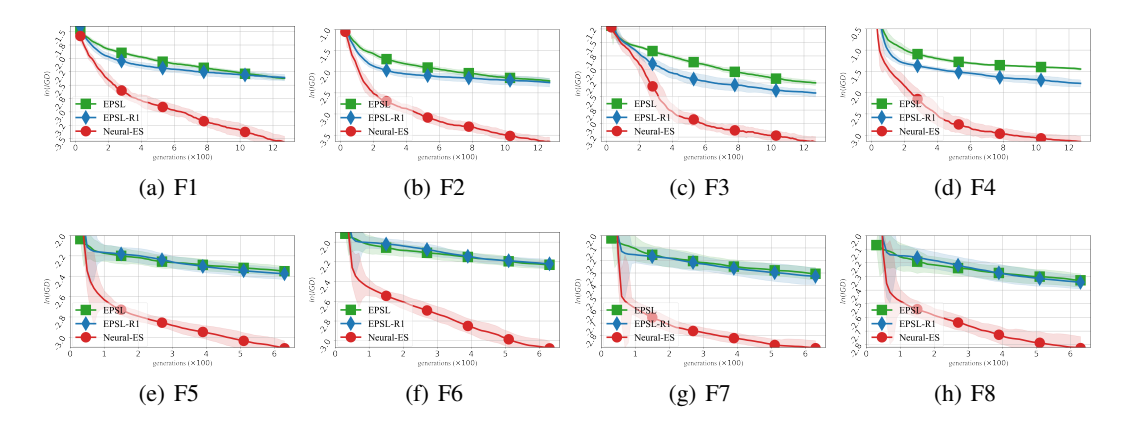


Figure 15: Convergence curves regarding the logarithm of the IGD values on the training solution sets, with n=256.

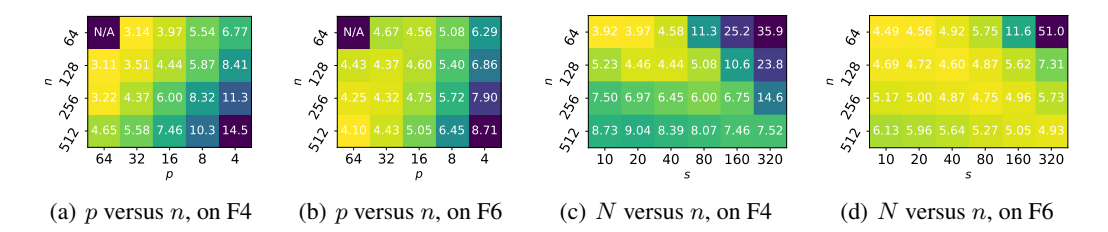


Figure 16: The acquired IGD values ($\times 10^{-2}$) in sensitivity analyses.

Table 3: Average training & testing IGD values ($\times 10^{-2}$) and standard deviations ($\times 10^{-3}$ in parentheses).

	n	LSO-CMO	IM-MOEA/D	EPSL	EPSL-R1	Neural-ES
	2^{5}	12.45 (47.98) —	5.141 (16.66)	7.202 (4.887) —	6.946 (11.16) —	$6.099_{(8.028)} =$
	2^{6}	15.77 (41.37) —	$5.570_{\ (19.31)} =$	$7.187_{(4.208)}$ $-$	8.216 (8.306) —	4.797 (8.051)
T7.1	2^{7}	20.38 (30.18) -	7.168 (21.02) $-$	8.252 (4.229) —	9.453 (8.892) $-$	3.997 (5.794)
F1	2^{8}	22.11 (22.86) —	$7.231_{(17.35)}$ $-$	9.758 (4.906) —	12.10 (7.956) —	3.967 (5.890)
	2^{9}	24.05 (9.820) —	8.082 (12.90) —	11.04 (3.594) —	14.74 (6.150) —	3.997 (4.171)
	2^{10}	26.62 (5.969) —	10.69 (9.372) —	12.71 (3.838) $-$	16.88 (6.946) —	5.336 (9.748)
	2^{5}	4.993 (17.41) =	6.526 (10.84) —	7.016 (8.088) —	4.588 (12.11)	5.457 (16.46) =
	2^{6}	6.739 (19.71) —	7.863 (14.81) $-$	$7.449_{(7.552)}$ $-$	6.588 (15.80) —	3.883 (11.72)
F2	2^{7}	8.445 (14.83) —	$8.726_{\ (12.97)}$ $-$	8.773 (4.078) —	7.581 (12.42) $-$	3.004 (3.696)
ГΖ	2^{8}	10.54 (12.55) -	9.788 (10.07) —	11.79 (7.447) —	11.95 (17.83) —	3.489 (5.859)
	2^{9}	15.13 (21.87) —	$13.20_{(34.25)}$ $-$	$13.59_{(4.785)}$ —	15.13 (13.01) —	3.727 (5.935)
	2^{10}	17.65 (16.18) —	$13.20_{\ (15.28)}$ $-$	17.05 (6.887) $-$	$19.12_{\ (12.04)}$ $-$	4.889 (5.704)
	2^{5}	$7.497_{\ (12.54)}$ $-$	13.52 (9.551) —	9.410 (7.694) —	6.629 (7.717)	$6.692_{(11.23)} =$
	2^{6}	9.351 (5.085) —	14.30 (4.552) $-$	9.486 (7.293) —	$7.477_{(9.134)}$ $-$	5.771 (8.698)
F3	2^{7}	11.83 (5.836) —	16.12 (4.709) $-$	10.63 (5.437) $-$	8.397 (7.823) —	5.986 (9.637)
1.3	2^{8}	14.24 (6.441) -	16.61 (4.133) $-$	11.68 (5.749) —	10.13 (8.249) —	5.863 (6.778)
	2^{9}	16.61 (8.691) —	16.66 (2.910) $-$	12.32 (5.782) $-$	12.81 (7.739) —	6.078 (4.259)
	2^{10}	19.13 (5.408) —	16.76 (1.821) $-$	14.22 (5.943) $-$	15.81 (9.210) —	6.654 (6.296)
	2^{5}	4.647 (39.09)	20.90 (13.96) —	15.85 (18.37) —	12.23 (13.27) $-$	6.561 (12.06) =
	2^{6}	8.420 (28.84) —	21.74 (11.57) $-$	14.44 (14.62) $-$	12.67 (18.09) $-$	5.685 (9.287)
F4	2^{7}	17.70 (33.43) —	23.77 (6.853) $-$	21.53 (9.107) $-$	15.71 (23.61) $-$	6.558 (10.62)
17	2^{8}	23.87 (15.02) —	24.73 (6.528) $-$	23.66 (7.163) —	19.13 (12.07) $-$	7.275 (8.371)
	2^{9}	27.69 (7.691) —	25.25 (4.206) $-$	24.64 (4.299) $-$	$22.88_{(15.45)}$ —	8.728 (8.730)
	2^{10}	$29.15_{(2.736)}$ —	25.42 (7.191) $-$	26.29 (5.367) —	26.65 (11.38) —	10.65 (10.97)
	2^{5}	4.190 (2.751) —	12.31 (12.62) —	7.233 (6.933) $-$	5.494 (6.135) —	3.261 (5.537)
	2^{6}	5.815 (4.487) —	$19.31_{\ (15.53)}$ —	8.065 (9.451) $-$	6.052 (6.118) $-$	3.090 (5.485)
F5	2^{7}	8.869 (7.198) —	24.87 (18.05) $-$	7.806 (6.459) $-$	$7.234_{(7.670)}$ –	2.793 (4.118)
	2^{8}	12.22 (17.98) —	32.98 (27.00) —	8.830 (6.493) —	7.982 (6.154) $-$	3.147 (3.708)
	2^{9}	14.39 (16.78) —	36.49 (21.15) $-$	8.976 (6.300) —	9.016 (11.79) $-$	3.370 (4.695)
	2^{10}	16.79 (21.62) —	39.58 (25.23) $-$	9.383 (6.579) —	9.764 (7.775) —	3.937 (4.777)
	2^{5}	4.528 (2.817) —	13.23 (13.22) $-$	7.454 (10.10) $-$	5.991 (6.928) —	2.752 (3.492)
	2^{6}	6.351 (5.353) $-$	20.27 (16.66) $-$	8.500 (8.668) —	7.368 (6.723) $-$	2.764 (3.685)
F6	2^{7}	9.792 (13.22) —	33.81 (129.79) $-$	8.930 (5.396) —	8.382 (8.728) —	2.635 (4.445)
	2^{8}	14.04 (23.30) —	32.74 (18.43) $-$	9.503 (4.951) —	9.297 (6.391) —	2.917 (3.655)
	2^9	18.06 (24.40) —	37.48 (18.25) —	10.10 (5.686) —	10.33 (6.855) —	3.261 (3.124)
	2^{10}	20.92 (41.97) —	39.94 (11.84) —	10.32 (4.974) —	11.31 (13.02) —	4.041 (4.753)
	2^{5}	4.633 (3.024) —	13.38 (17.32) —	7.998 (6.516) —	5.918 (4.893) —	4.026 (6.118)
	2^{6}	6.498 (5.846) —	18.77 (16.75) $-$	8.120 (7.429) —	6.694 (4.773) $-$	4.166 (3.573)
F7	2^7	9.592 (13.00) —	28.54 (50.67) —	8.581 (4.237) —	7.147 (5.947) —	4.213 (3.333)
	2^{8}	12.69 (17.88) —	31.79 (17.96) —	9.277 (7.330) —	8.386 (7.677) —	4.330 (2.266)
	2^9	17.31 (27.64) —	34.64 (12.73) —	9.585 (6.458) —	9.084 (7.185) —	4.523 (2.586)
	2^{10}	21.01 (23.59) —	37.25 (17.04) —	9.726 (5.192) —	9.935 (8.296) —	4.833 (1.760)
	$\frac{2^5}{2^6}$	4.833 (3.210)	12.41 (22.91) —	7.790 (7.609) —	6.726 (7.825) —	5.105 (5.517) =
	$\frac{2^6}{2^7}$	6.765 (5.986) —	18.51 (12.94) —	8.413 (9.989) —	6.936 (5.334) —	4.472 (4.858)
F8	$\frac{2^7}{2^8}$	9.127 (8.242) —	25.61 (22.68) —	8.663 (7.097) —	7.340 (5.793) —	4.220 (3.594)
	$\frac{2^8}{2^9}$	12.44 (14.13) —	30.38 (15.34) —	9.471 (7.997) —	8.243 (6.328) —	4.347 (3.694)
	$\frac{2^9}{2^{10}}$	16.69 (22.96) —	34.29 (16.27) —	9.076 (5.806) —	8.655 (5.327) —	4.477 (2.702)
	210	19.06 (42.91) —	36.74 (17.06) —	9.462 (4.698) —	9.316 (5.610) —	4.939 (3.172)